



Review

Application of Defect Engineering via ALD in Supercapacitors

Tiange Gao ¹, Xiaoyang Xiao ¹, Zhenliang Dong ¹, Xilong Lu ¹, Liwen Mao ¹, Jinzheng Wang ¹, Yiming Liu ^{2,*}, Qingmin Hu ^{1,*} and Jiaqiang Xu ¹

¹ New Energy and Sensing Technology (NEST) Lab, Department of Chemistry, College of Sciences, Shanghai University, Shanghai 200444, China

² Future Battery Research Center, Global Institute of Future Technology, Shanghai Jiaotong University, Shanghai 200240, China

* Correspondence: liuyiming-sjtu@sjtu.edu.cn (Y.L.); huqingmin@shu.edu.cn (Q.H.)

Abstract: Supercapacitors are a kind of energy storage device that lie between traditional capacitors and batteries, characterized by high power density, long cycle life, and rapid charging and discharging capabilities. The energy storage mechanism of supercapacitors mainly includes electrical double-layer capacitance and pseudocapacitance. In addition to constructing multi-level pore structures to increase the specific surface area of electrode materials, defect engineering is essential for enhancing electrochemical active sites and achieving additional extrinsic pseudocapacitance. Therefore, developing a simple and efficient method for defect engineering is essential. Atomic layer deposition (ALD) technology enables precise control over thin film thickness at the atomic level through layer-by-layer deposition. This capability allows the intentional introduction of defects, such as vacancies, heteroatom doping, or misalignment, at specific sites within the material. The ALD process can regulate the defects in materials without altering the overall structure, thereby optimizing both the electrochemical and physical properties of the materials. Its self-limiting surface reaction mechanism also ensures that defects and doping sites are introduced uniformly across the material surface. This uniform defect distribution is particularly profitable for high surface area electrodes in supercapacitor applications, as it promotes consistent performance across the entire electrode. This review systematically summarizes the latest advancements in defect engineering via ALD technology in supercapacitors, including the enhancement of conductivity and the increase of active sites in supercapacitor electrode materials through ALD, thereby improving specific capacitance and energy density of the supercapacitor device. Furthermore, we discuss the underlying mechanisms, advantages, and future directions for ALD in this field.



Citation: Gao, T.; Xiao, X.; Dong, Z.; Lu, X.; Mao, L.; Wang, J.; Liu, Y.; Hu, Q.; Xu, J. Application of Defect Engineering via ALD in Supercapacitors. *Batteries* **2024**, *10*, 438. <https://doi.org/10.3390/batteries10120438>

Academic Editor: Leon L. Shaw

Received: 14 November 2024

Revised: 29 November 2024

Accepted: 6 December 2024

Published: 10 December 2024



Copyright: © 2024 by the authors. Licensee MDPI, Basel, Switzerland. This article is an open access article distributed under the terms and conditions of the Creative Commons Attribution (CC BY) license (<https://creativecommons.org/licenses/by/4.0/>).

1. Introduction

The rise of the global economy, coupled with fossil resource depletion and environmental pollution, has led to a growing emphasis on sustainable development and renewable energy sources like solar, hydropower, and wind energy. However, despite their potential, the intermittent nature of these energy sources highlights the ongoing challenge of effective electricity storage and supply [1–3]. Among various energy storage devices, batteries and supercapacitors (SCs) are two advanced electrochemical energy storage technologies. High-energy-density lithium-ion batteries (LIBs) have been widely commercialized and applied in various electronic products and new energy vehicles. However, due to their high cost, low charge/discharge rates, low electron and ion transport, and dendrite problems during high-power operation, the applications of LIBs are limited. Supercapacitors can safely provide fast charging and an ultra-long cycle life (>100,000 cycles), making them capable of compensating for or even replacing lithium-ion batteries in certain fields [4–9]; the significance of supercapacitors is shown in Figure 1a. However, the energy density of

supercapacitors is significantly lower than LIBs and fuel-cells, as shown in Figure 1b [10]. Therefore, increasing the energy density of the supercapacitor without sacrificing the power density and cycle stability is the key to its further application.

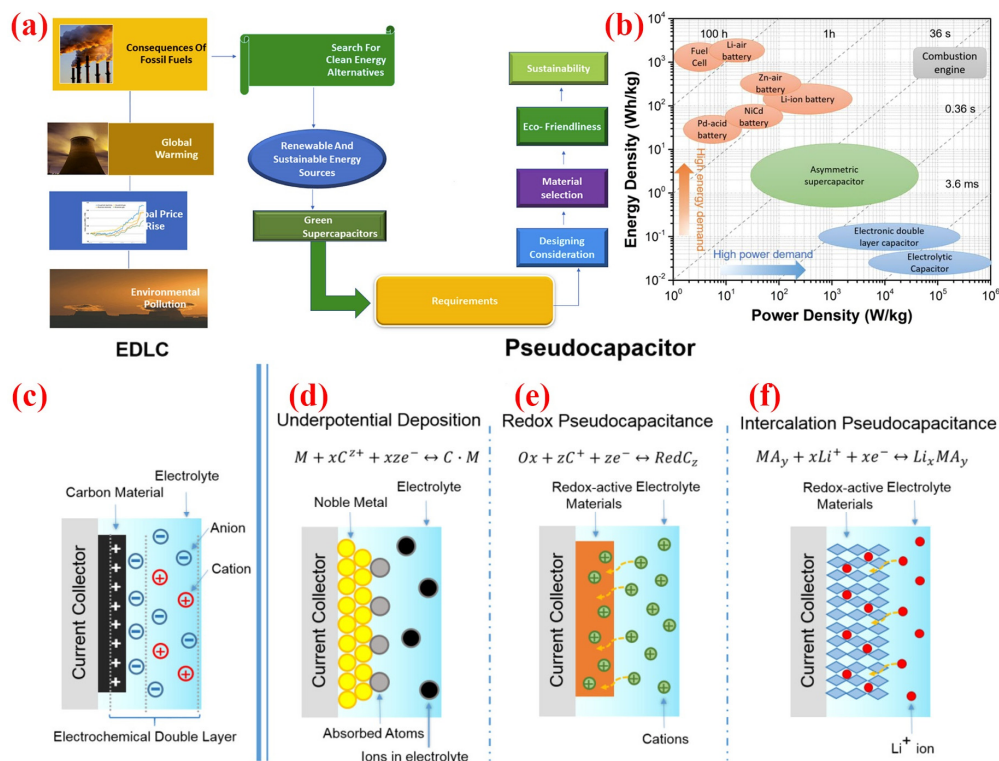


Figure 1. (a) Graphical illustration portraying the requisites for green supercapacitors and aspects associated with their development. Reproduced with permission. Copyright 2024, Elsevier Publishing [4]. (b) Ragone plot illustrating the performances of specific power vs. specific energy for different electrical energy-storage technologies. Schematics of charge-storage mechanisms for (c) an EDLC. Reproduced with permission. Copyright 2018, ACS Publishing [10]. (d–f) Different types of pseudocapacitive electrodes: (d) underpotential deposition, (e) redox pseudocapacitor, and (f) ion intercalation pseudocapacitor. Reproduced with permission. Copyright 2014 Royal Society of Chemistry [11].

The energy storage mechanisms of supercapacitors can be categorized into two types, as illustrated in Figure 1c–f [10,11]: electrical double-layer capacitance (EDLC) and pseudocapacitance. When electrode materials are immersed in an electrolyte, due to electrostatic interaction, charges spontaneously migrate in a directional manner towards the two electrodes, forming charge layers, as shown in Figure 1c. These charge layers, together with the electrode plates, constitute the electrical double layer. In this process, there is no charge transfer, and charge storage relies on electrostatic charge adsorption. The specific capacitance of EDLC primarily depends on the specific surface area and surface properties of the material. In contrast to EDLC, pseudocapacitive electrode materials store charges through rapid and reversible Faraday reactions occurring on or near the surface, relying on changes in elemental valence states, which result in electron transfer. The mechanisms of pseudocapacitance are primarily categorized into three types: underpotential deposition, redox reactions, and ion intercalation. Underpotential deposition is commonly observed in the adsorption of hydrogen atoms by noble metals with catalytic properties, as shown in Figure 1d. In Figure 1e, the pseudocapacitive electrode materials based on redox reactions exhibit electron transfer between oxidized and reduced states during energy storage. Specifically, the oxidized surface undergoes electrochemical adsorption of cations accompanied by rapid and reversible electron transfer. Pseudocapacitance also involves the insertion and

extraction of ions, as shown in Figure 1f. Despite differing energy storage mechanisms, the above three pseudocapacitive systems exhibit similar electrochemical characteristics. This is attributed to the identical relationship between the potential and coverage of electrolyte ions on or near the material surface during charging and discharging, which results in a higher charge storage capacity on the material surface compared to that of EDLC.

Electrode materials are crucial for supercapacitors, but they are largely limited by poor reaction kinetics, resulting in suboptimal performance [12,13]. Therefore, developing electrode materials with robust reaction kinetics is of great significance. Currently, the main problems we are facing encompass two aspects. Firstly, metallic oxides lack an efficient electron transport path and electron/ion transfer interface, thus obtaining a slow rate capability [14,15]. In addition, the volume contraction/expansion during the charging and discharging process causes the electrode to shatter, resulting in decreased stability [16,17]. In the past few decades, people have designed and prepared electrode materials with high reaction kinetics using various methods, including integrating conductive substrates to improve conductivity [18,19], preparing porous structures to increase surface area [20,21], and constructing heterostructures and surfactant functional groups as electrochemical reaction sites. However, the improvement in reaction kinetics of supercapacitors is quite limited, as this “external” approach cannot eliminate the intrinsic property limitations of materials.

Among various design strategies, defect engineering, as an “intrinsic regulation” method, can effectively regulate the intrinsic properties of electrode materials to promote their reaction kinetics and thus achieve excellent electrochemical performance [22–24]. Taking energy density as an example, the introduction of defects, such as oxygen vacancies or metal doping, can increase the carrier concentration in materials, thereby enhancing their electrical conductivity. The improvement in electrical conductivity aids in reducing the internal resistance of supercapacitors during charging and discharging processes, thus elevating their energy density. Furthermore, the incorporation of defects creates additional ion diffusion pathways and electrochemical active sites. The former helps shorten the response time of supercapacitors during charging and discharging, while the latter facilitates charge storage and release, thereby further enhancing the energy density of supercapacitors. Many studies now aim to achieve faster reaction kinetics through defect engineering, thereby improving electrochemical performance [25–27]. For example, Fu et al. successfully constructed a yolk-shell structured MnO₂ microsphere with oxygen vacancies through a simple three-step method. The obtained MnO₂ microspheres possess superior conductivity, which can accelerate the diffusion of electrolyte ions, leading to higher specific capacitance (the specific capacitance of ov-MnO₂ is twice that of pure MnO₂) and high energy density (40.2 Wh kg⁻¹) [28]. Yang et al. proposed a strategy to generate oxygen vacancies in MoO_{3-X} to achieve larger interlayer spacing with improved charge storage kinetics. Oxygen vacancies can not only significantly increase the interlayer spacing and conductivity of MoO₃, but also greatly enhance its electrochemical activity; the fabricated asymmetric supercapacitor exhibits an ultrahigh energy density of 150 Wh kg⁻¹ [29]. Li et al. have demonstrated that doping Cu into Ni₃S₂ could introduce defect energy levels near the fermi level to enhance intrinsic electronic conductivity and electrochemical activity, which helps to accelerate the kinetics of redox reactions, thereby exhibiting high energy density (33.7 Wh g⁻¹ at 850.1 W kg⁻¹) and long cycle stability (the retention after 5000 cycles is 94.0%) [30].

Atomic layer deposition (ALD) technology is an advanced method that utilizes the principle of chemical vapor deposition to deposit materials layer by layer on a substrate surface through precise control of chemical reactions [31,32]. The core of this technology lies in its self-limiting growth characteristics, where each chemical reaction occurs only on a single layer of atoms/molecules, thereby achieving precise control on the thickness and composition of the as-prepared thin film [33,34]. This means that ALD can accurately introduce defects into different material systems, such as metals, semiconductors, insulators, organic materials, etc. This means that we can design a general defect engineering method

based on ALD for the selection of the most suitable materials as needed to introduce or repair defects [35–37]. In addition, ALD technology has shown great potential in designing and engineering high-performance electrode materials. As a unique thin film deposition technology, ALD achieves precise thickness control and excellent deposition quality through self-terminating surface reactions, which is crucial for optimizing the performance of supercapacitor electrode materials [38–40].

In this review, we first introduced the history, principles, and wide applications of ALD in various fields. Subsequently, the application of ALD in defect engineering is reviewed, including the use of ALD technology to manufacture oxygen vacancies, surface defects, and passivation of defects. The unique advantages of ALD in defect engineering are analyzed. Finally, the application of ALD in supercapacitors is introduced, including the preparation of supercapacitor electrode materials and their defect engineering using ALD technology.

2. Introduction of ALD

Atomic layer deposition (ALD) is a high-precision thin film preparation technique. In the 1970s, ALD technology was first referred to as atomic layer epitaxy (ALE) when it was used to deposit ZnS thin films on flat display panels [41]. Since the beginning of the 21st century, continuous, self-limiting surface reactions have been introduced into the process of thin films, no longer requiring epitaxial growth to their underlying substrates [42]. Modern ALD technology has made considerable progress and became a mature scientific technology. ALD relies on continuous self-limiting surface reactions to deposit thin films layer by layer on the material surface, achieving atomic level control accuracy [36,43–46]. This technology allows the introduction of chemical precursors (mainly gaseous compounds) into the reaction chamber to interact with specific adsorption layers on the substrate surface, and then effectively remove unreacted precursors and reaction by-products through inert carrier gas blowing. This process will be repeated until the desired film thickness, composition, and structure is achieved [37,47–49].

The reaction mechanism of ALD technology is grounded in a self-limiting surface reaction [50,51]. In each reaction cycle, the precursor only reacts with the reactive sites available on the surface, forming a monolayer of material, after which the reaction ceases spontaneously until the subsequent precursor is introduced. This self-limiting attribute guarantees the uniform deposition of atoms layer by layer, thereby achieving precise control over the thickness of the thin film [52–54]. Figure 2 visually illustrates the ALD process of SnN_x ; the deposition process is divided into two and a half reactions [55].



Substances transferred or anchored onto substrates through chemical adsorption are marked with asterisks (*). Reactions (1) and (2) are both ammonia exchange reactions, where the surface material of NH_x^* is replaced by the surface material of $\text{Sn}(\text{N}(\text{CH}_3)_2)_y^*$.

The core advantage of ALD technology depend on its self-limiting growth characteristics [56–58]. This self-limiting property enables ALD to grow highly uniform conformal films on three-dimensional structures while achieving atomic level growth and regulation [59–61]. ALD possesses the properties of sequential, self-limiting, and controllable surface reactions, allowing thin films to grow conformally and atomically on various substrates. The key features of ALD include excellent thickness control, high uniformity, and the ability to coat complex geometries, which are attributed to the self-limiting growth mechanism where each cycle deposits a predictable amount of material [62]. The low temperature processing capabilities of ALD make it suitable for a wide range of materials [63], including thermally sensitive substrates, while the layer-by-layer growth enables the engineering of nanolaminates and multifunctional coatings with tunable properties. Moreover, the high aspect ratio gap filling is another notable advantage of ALD, which is crucial for advanced semiconductor devices and nanoelectronics [64,65]. These distinc-

tive characteristics of ALD have positioned it as a pivotal technology in fields such as microelectronics, energy storage and conversion, and surface modification [66,67].

ALD has found widespread applications across various industries due to its ability to deposit high-quality, conformal, and ultrathin films with precise control over thickness and composition. ALD plays a pivotal role in the development of transparent conductive oxides (TCOs) for solar cells, where it contributes to enhanced light transmission and reduced resistance [43,68]. Moreover, in the realm of energy storage, ALD is employed for the coating of battery electrodes to improve cycling stability and capacitance, with applications ranging from lithium-ion batteries to emerging battery technologies like sodium-ion and solid-state batteries [69]. Additionally, the catalysis field benefits from ALD for the preparation of well-defined catalysts with enhanced activity and selectivity, which is crucial for chemical synthesis and environmental protection [70,71]. These applications underscore the versatility and importance of ALD in enabling advanced technologies across multiple sectors.

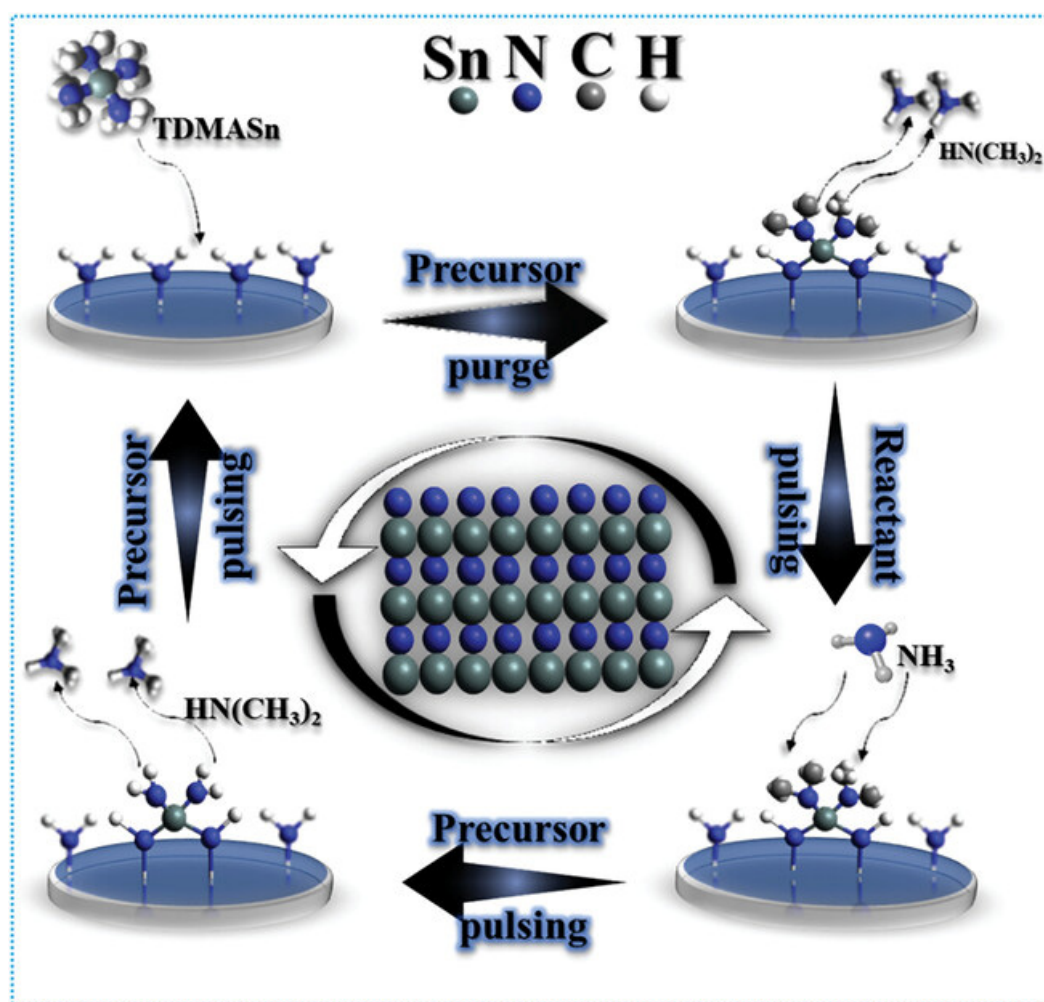


Figure 2. Schematic of ALD of tin nitride (SnN_x) process using TDMA_{Sn} and NH_3 precursors as an example. Reproduced with permission. Copyright 2023, Wiley-VCH [55].

3. ALD for Defect Engineering

ALD technology plays a pivotal role in defect engineering. By precisely controlling the deposition process, it forms uniform and dense thin films on material surfaces at the atomic level, effectively modifying and reducing surface defects. This technology not only exhibits high step coverage, ensuring the formation of continuous films on complex or irregular surfaces, but also features low-temperature deposition, thereby avoiding the adverse effects

of high-temperature processing on material properties. Compared with other technologies, ALD has unique advantages in defect engineering. Chemical vapor deposition (CVD) is a common synthesis method, whose principle primarily involves the utilization of gaseous substances to induce chemical reactions and transport reactions on solids at high temperatures, resulting in the formation of solid deposits. This technique is widely applied in various fields. However, in some reactions, excessively high temperatures can lead to the disappearance of defects [72]. In contrast, ALD is typically conducted at low temperatures, effectively avoiding such issues. Solvent-phase synthesis has been demonstrated to be capable of preparing electrode materials containing defects [73,74]. However, solvents may pose environmental and safety concerns, and separating and purifying products from solutions may require additional steps, such as evaporation, extraction, and crystallization, which can increase costs and time [75]. ALD, on the other hand, can be performed without the use of solvents and can achieve a more uniform distribution of defects.

3.1. ALD for Oxygen Vacancy Engineering

ALD technology alternately introduces precursor gas and reactant gas to perform chemical reactions on the substrate surface, forming a single-layer film. During the reaction process, the concentration and distribution of oxygen vacancies in the thin film can be controlled by adjusting type of precursor, temperature and gas partial pressure during the deposition process [76,77]. It possesses the advantages of high precision, good uniformity, and strong controllability. Thin films with specific oxygen vacancy concentrations prepared by ALD technology have shown excellent performance and broad application prospects in fields such as photocatalytic materials, perovskite solar cells, and supercapacitors [78–80].

3.1.1. ALD for Bulk Phase Oxygen Vacancy

Transition metal oxides with abundant oxygen vacancies can be grown via ALD on substrates by tuning deposition parameters. For example, Wang et al. synthesized corrosion-resistant thin films rich in oxygen vacancies on Al substrates by controlling the blowing time and pulse ratio of $\text{TiCl}_4/\text{H}_2\text{O}$ (Figure 3a). As shown in Figure 3b, The O/Ti ratio of TiO_2 would change accordingly through controlling the $\text{TiCl}_4/\text{H}_2\text{O}$ pulse ratio in order to regulate the content of oxygen vacancies in different TiO_2 samples. In corrosion testing, as shown in Figure 3c, the sample coated with a TiO_2 coating layer rich in oxygen vacancies has a higher corrosion barrier, meaning that the leaching of Al in the underlying matrix is reduced, and the corrosion resistance is the best [81]. Li et al. grew ZnO thin films directly on SiO_2/Si chips using ALD and then subjected the ZnO thin films to Ar treatment, as shown in Figure 3d. XPS analysis showed that the ZnO thin films grown directly using ALD contained abundant oxygen vacancies, and the concentration of oxygen vacancies could be further controlled through Ar treatment (Figure 3e). The atomic structure diagram of ZnO thin film is shown in Figure 3f. There are both oxygen vacancies and internal defects on the ZnO surface, and the content of oxygen vacancies is usually directly related to the gas sensing performance [82]. The test shown in Figure 3g also proves that the sample (noted as 700) with the highest concentration of oxygen vacancies exhibits the best gas sensing performance. Subsequently, the mechanism was explained in detail (Figure 3h). The abundant oxygen vacancies increase the concentration of adsorbed oxygen, allowing more gas molecules to adsorb on the surface to promote subsequent redox reactions. In addition, oxygen vacancies act as electron donors, increasing the charge density of the maximum valence band and minimum conduction band in the vicinity. This is due to the reduced bandgap of ZnO , which is conducive to the adsorption and activation of TEA. Therefore, it exhibits excellent sensing performance for TEA [83].

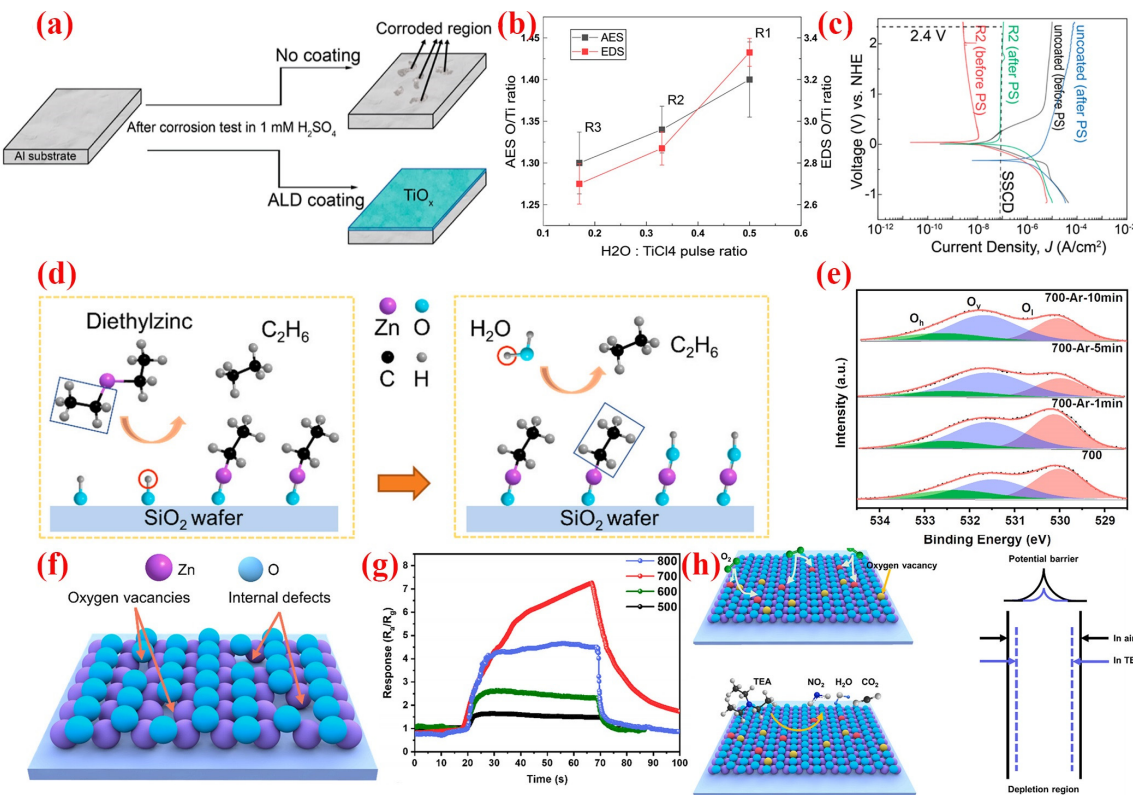


Figure 3. (a) Schematic outline of the corrosion protection of Al substrate achieved by optimized ALD TiO_x protection layers; (b) O/Ti ratios for the ALD recipes; (c) polarization curves. Reproduced with permission. Copyright 2024, ACS Publishing [81]. (d) ALD deposition process of ZnO; (e) XPS survey spectra of ZnO films; (f) atomic structure of oxygen-deficient ZnO surface; (g) gas sensing test; (h) surface reaction mechanism. Reproduced with permission. Copyright 2021, Elsevier Publishing [83].

3.1.2. ALD for Interface/Surface Oxygen Vacancy

The ALD process is a technology from bottom to top that enables precise adjustment of surfaces and interfaces [84,85]. Therefore, in addition to directly generating metal oxides containing oxygen vacancies, oxygen vacancies can also be constructed at the interface between two thin films. For example, Hu et al. modified ZnO on HKUST-1 via ALD and calcined it to form Cu-doped ZnO (CZO-6) with a core–shell structure, as shown in Figure 4a. As shown in Figure 4b, the oxygen vacancies generated at the Zn-O-Cu interface can act as adsorption sites for hydrogen sulfide, further improving selectivity and sensitivity. This has also been demonstrated in the gas sensing testing (Figure 4c) [86]. Similarly, Hu et al. used ALD to modify the CoO_x surface of ZnO thin films and deposited ultra-thin ZnCo_y gas sensitive films (Figure 4d). Due to the different deposition cycles, it was observed from Figure 4e,f that Co elements were uniformly distributed in the form of particles with a diameter of 5 nm on the surface of ZnO thin films. As shown in Figure 4g,h, XPS analysis showed that the addition of Co increased the oxygen vacancy content at the Co-O-Zn interface, and the synergistic effect of abundant oxygen vacancies and heterojunction interface sites increased the surface oxygen content and H₂S selective oxidation to S, which is consistent with the gas sensing test results, as shown in Figure 4i,j [87]. In addition, unlike traditional immersion or drop coating thin films, ALD ZnO thin films have a compact structure, which is not only beneficial for improving sensing performance but also plays an important role in the field of energy storage [88–91].

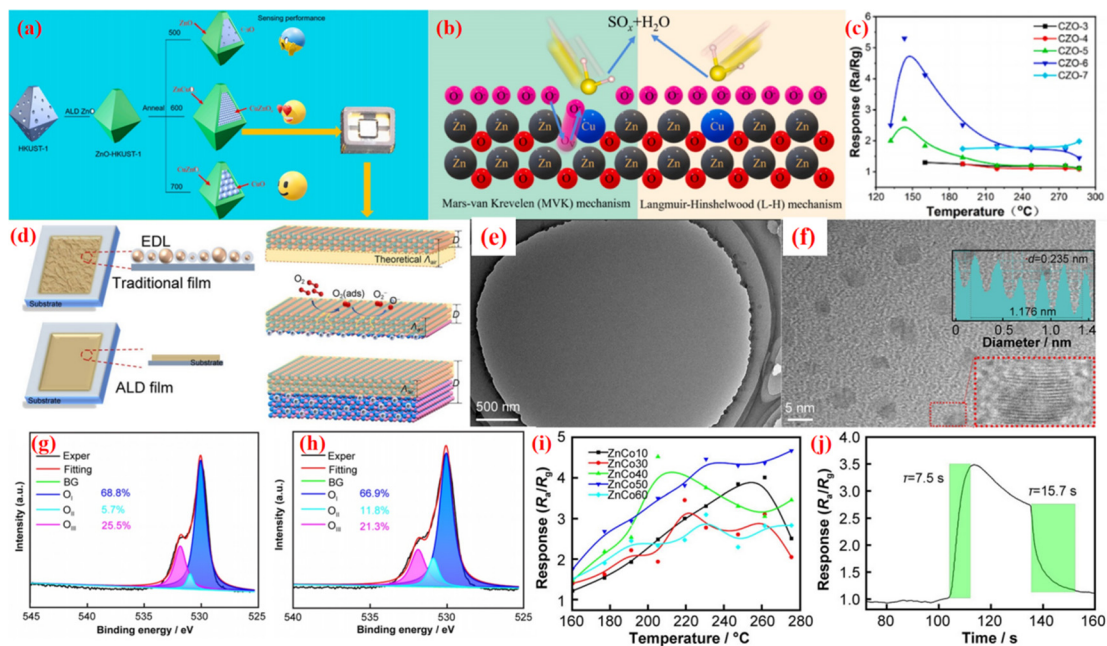


Figure 4. (a) Schematic diagram of the formation process of confined samples; (b) the schematic illustration for proposed sensing mechanism; (c) sensing performance. Reproduced with permission. Copyright 2024, Elsevier Publishing [86]. (d) Illustration of intergranular contact regions and relation between ALD ZnO thickness and length of space-charge layer; (e,f) TEM and HRTEM images. XPS survey spectra of (g) ZnO films and (h) ZnCo50 film; (i,j) gas sensing test. Reproduced with permission. Copyright 2023, Springer Nature Publishing [87].

3.1.3. ALD for Inside Oxygen Vacancy

Oxygen vacancies in samples fabricated with ALD techniques are not only present at the interfaces between different oxide layers or on the surface of the materials but also can be generated inside the hollow structure. This usually requires the active species, such as zeolites [92], carbon nanotubes [93], and metal–organic frameworks (MOFs), to be confined in nanometer or subnanometer spaces [94] to create a unique microenvironment, thereby regulating the rate and path of chemical reactions. This is also known as spatial confinement and is widely used to improve the activity and selectivity of catalysts. Dong et al. deposited Pt nanoparticles into the pores of SnO₂ using the ALD method, as shown in Figure 5a. The closed separation of Pt sites accelerates the adsorption of acetone and the redox reaction between acetone and adsorbed oxygen, thus exhibiting excellent sensing performance (Figure 5b). XPS analysis also showed that the addition of Pt increased the concentration of oxygen vacancies, proving that oxygen vacancies were generated inside the material by the ALD method (Figure 5c). The DFT calculation shown in Figure 5d indicates that acetone molecules are more easily adsorbed on SnO₂-Pt2. The closed structure increased the concentration of acetone, and the synergistic effect of Pt separation catalysis and the restricted structure significantly improved the sensing performance, which is also reflected in Figure 5e [95]. Hu et al. used the sacrificial template method to deposit Ni and Sn species in different orders on the surface of carbon nanotubes, followed by calcination to remove carbon, resulting in NiO-SnO₂ nanocoils (NiSnNCs), as shown in Figure 5f. Depending on the location of Ni, they were labeled as outside NiSnNCs (O-NiSnNCs), inside NiSnNCs (I-NiSnNCs), and both outside and inside NiSnNCs (B-NiSnNCs). The position of Ni in different samples can be accurately observed from TEM images, shown in Figure 5g. The XPS results also indicate that the generation of oxygen vacancies can be controlled outside, inside, or both inside and outside the hollow tube, depending on the location of Ni, with I-NiSnNCs having the highest proportion of oxygen vacancies (Figure 5i–k). The high sensing performance of confined NiO in SnO₂ nanocoils is due to the overflow of dissociated H on NiO to the interface active sites, as well as the synergistic effect of

NiO and SnO_2 , leading to the enrichment of hydrogen concentration. This phenomenon is called the funnel effect [96].

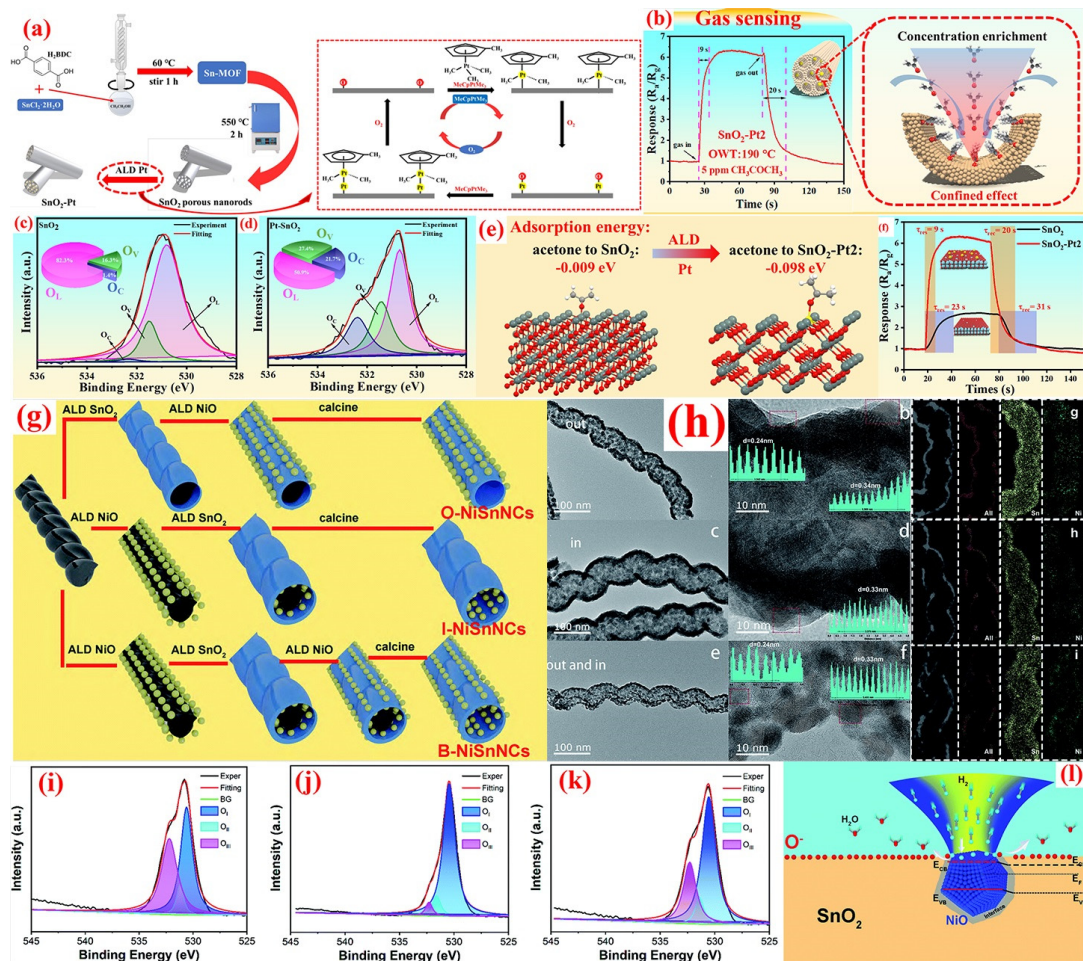


Figure 5. (a) Synthesis route of SnO_2 porous nanorods; (b) the scheme of detection of VOCs and the sensing performance; (c,d) XPS survey; (e) the adsorption of acetone molecules; (f) the response transient. Reproduced with permission. Copyright 2024, Elsevier Publishing [95]. (g) Schematic illustration of the fabrication of NiSnNC samples; (h) TEM and HRTEM images; (i–k) XPS survey spectra of O-NiSnNCs, I-NiSnNCs, and B-NiSnNCs. (l) The funnelling effects of the hydrogen concentration effects during the sensing performance. Reproduced with permission. Copyright 2022, RSC Publishing [96].

In summary, not only samples containing oxygen vacancies can be directly prepared, but oxygen vacancies can also be formed at the interface between layers through multiple deposition through ALD. In addition, for some specific situations, the generation location of oxygen vacancies can have a significant impact on the entire reaction. Through the controllability of ALD technology, it is possible to generate oxygen vacancies at specific locations.

3.2. ALD for Surface Defect

Surface defect engineering is a technique that introduces or controls defects on the surface of materials to improve their performance, significantly affecting the electronic structure and surface properties of the materials [97,98]. It demonstrates its unique value and potential in various fields, such as catalysis, energy conversion, electrochemical sensing, and environmental protection [99–101]. Surface defect engineering can be achieved through methods such as chemical vapor deposition (CVD), laser processing, and ion implanta-

tion [102–104]. ALD can adjust atomic stoichiometry and doping levels in self-limiting surface reactions, thereby obtaining unique conformal and pinhole free films, which can play an important role in surface defect engineering [105].

Yu et al. altered the density of Ni vacancy (V_{Ni}) defects in bulk NiO_x by adjusting the oxygen injection time (t_{OE}) during the ALD process, as shown in Figure 6a–d. The Ni-O bond is disrupted to a varying degree by O_2 plasma; the ratio of Ni^{3+}/Ni^{2+} and O/Ni increase with the increase of oxygen injection time, indicating that the content of surface Ni defects (V_{Ni}) is proportional to the oxygen injection time (Figure 6e,f). The alteration in Ni defects concentration fine-tunes the physical and chemical properties of NiO_x thin films, improving carrier transport as well as reducing adverse redox reactions at the PVK/ NiO_x interface. And that also increased power conversion efficiency (PCE) from 18.19% to 19.86%, shown in Figure 6g,h [106]. Dai et al. deposited an additional TiO_2 layer on the surface of TiO_2 nanowire film (TNF) using ALD. The structure of ALD TiO_2 undergoes a transition from ordered to completely disordered. The presence of Ti^{3+} defects in the ALD TiO_2 layer can be confirmed from XPS results. The effective ion diffusion coefficient of the electrode can be enhanced by increasing the thickness of the ALD TiO_2 layer, and the electrochemical performance of ALD TiO_2 modified TNF is significantly improved. The deposition of an additional TiO_2 layer on crystalline TiO_2 nanowire thin film by the ALD modification method comprehensively improves electrochemical performance, as its surface structure continuously evolves, including interconnected domains, Ti^{3+} defects, and exchangeable hydroxyl groups, thereby comprehensively enhancing the electrochemical performance of TiO_2 nanowire film [107].

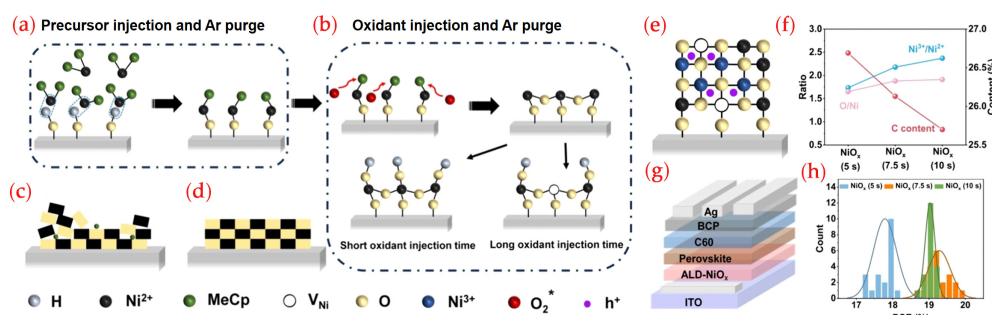


Figure 6. (a–d) Schematic illustration of the principle of modulating the valence state of the Ni element using ALD; (e) schematic NiO_x lattice structure with Ni vacancy defects; (f) surface O/ni ratio, Ni^{3+}/Ni^{2+} ratio, and C content of different NiO_x ; (g) schematic stack of the p-i-n structured PSCs; (h) PCE histograms of 20 devices. Reproduced with permission. Copyright 2024, ACS Publishing [106].

3.3. ALD for Passivation of Defect

In some fields, the appearance of defects often leads to a decline in material properties, and the formation of defects is inevitable in the material preparation process. Repairing or passivating defects can improve material properties. Defect passivation is a technique that introduces or regulates defects on the surface of materials to improve their performance [108,109]. This technology has demonstrated its unique value and potential in multiple fields such as catalysis, energy conversion, electrochemical sensing, and environmental protection [110–113]. Taking perovskite solar cells as an example, the presence of defects can lead to energy loss, ion migration, operational instability, and hysteresis, seriously hindering their potential for industrial applications. Therefore, researchers have developed various defect passivation strategies, including using additives to passivate defects in perovskite materials [114]. These strategies involve surface modification of materials as well as control of internal defects to reduce nonradiative recombination, charge capture and scattering, ion migration, and other phenomena.

ALD has unique advantages in defect passivation, especially in improving material performance and stability. ALD technology can perform thin film growth at lower tem-

peratures, which helps to protect the substrate material from thermal damage and reduce the occurrence of thermally induced defects [115]. And ALD technology can also deposit various materials, including metals, semiconductors, insulators, and organic materials. This multifunctionality enables ALD technology to select suitable materials for surface defect passivation according to different application requirements [116]. For example, Ng et al. reported the use of the ALD method to coat 3D-printed nanocarbon surfaces, as shown in Figure 7a. Figure 7b displays the 3D electrode surface morphology of an 80 ALD cycle Al_2O_3 coating at different magnifications. Owing to the extremely thin nanoscale coating, scanning electron microscopy (SEM) imaging of the carbon surface of Al_2O_3 coating was performed using a high angle annular dark field (HAADF) detector with 20 and 80 ALD cycles. The initial growth of Al_2O_3 in the 20th cycle is characterized by unevenly sized islands dispersed on the surface. As the ALD process continues and the number of cycles increases, the deposited islands become additional nucleation sites for subsequent growth. These islands combine to form larger islands and expand into adjacent uninhabited spaces. Therefore, 80 cycles of Al_2O_3 produced larger and thicker island layers, gradually forming a more continuous coating, which confines the initial nucleation at the defect sites and edges as anchoring sites. Figure 7c reveals SECM images of electrocatalytic oxidation for blank and 80 cycle Al_2O_3 -coated 3D-printed nanocarbon electrodes. At the same voltage, 80 cycle Al_2O_3 exhibits a stronger current, and the Al_2O_3 coating can catalyze the oxidation of catechol, which is further confirmed by Figure 7d,e. Al_2O_3 -coated 3D-printed nanocarbon electrodes exhibit superior electrochemical performance. The thin Al_2O_3 film deposited on the electrode can not only effectively serve as an active layer for adsorbing catechins but also serve as a surface passivation layer to reduce the defect density inside the carbon fiber electrode [117].

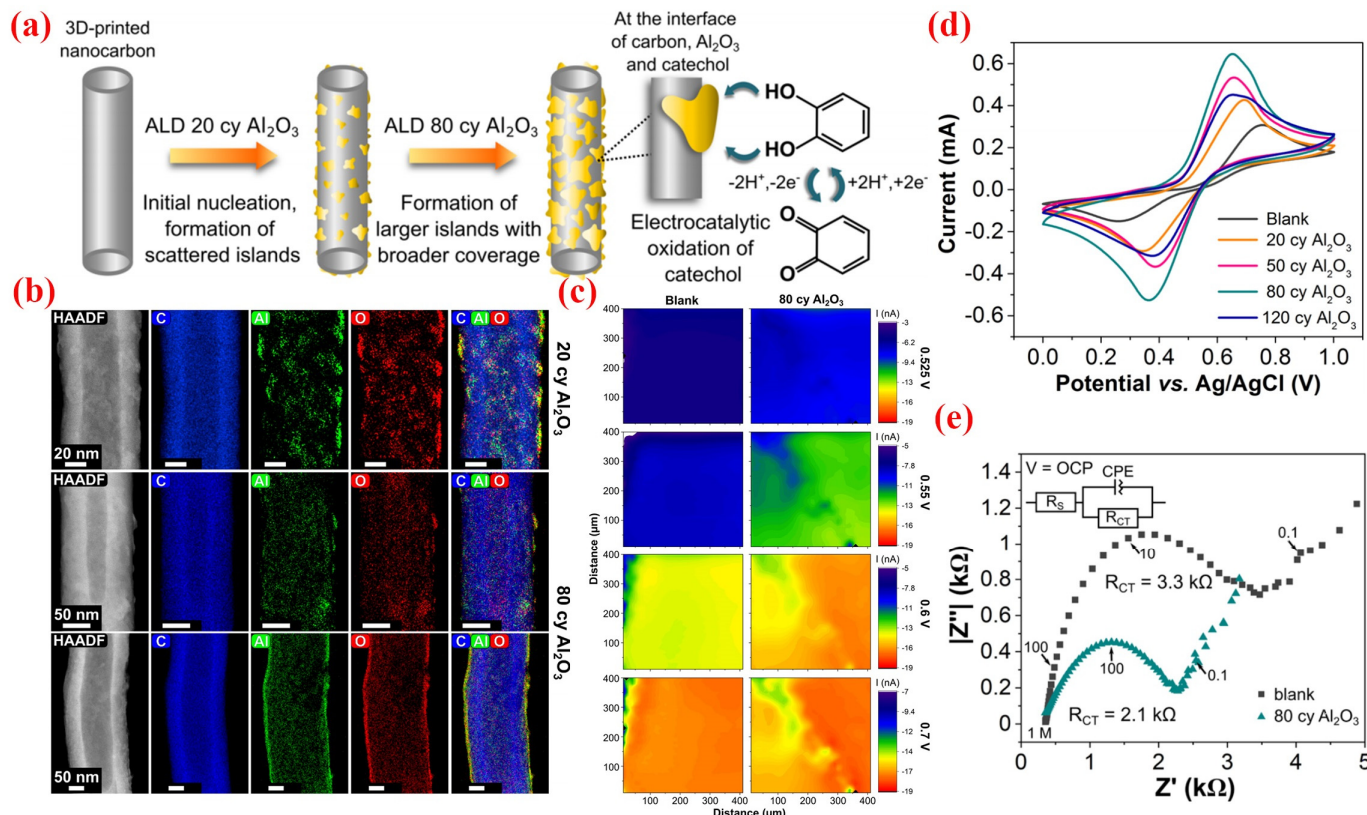


Figure 7. (a) Mechanism of the electrocatalytic oxidation of catechol to o-benzoquinone; (b) STEM-HAADF images; (c) SECM images of electrocatalytic oxidation acquired via substrate generation/tip collection (SG/TC) mode for blank and 80 cycle Al_2O_3 -coated 3D-printed nanocarbon electrodes; (d,e) electrochemical characterization. Reproduced with permission. Copyright 2021, ACS Publishing [117].

4. Defect Engineering via ALD for Supercapacitors

4.1. ALD for Supercapacitors

Electrochemical supercapacitors have become one of the most promising strategies for the next generation of energy storage systems due to their high-power density, fast charging and discharging rates, significant cycling stability, and low maintenance costs [118–121]. Generally speaking, capacitance electrodes with high power capacity require high surface area and good conductivity to form double layers and undergo redox reactions. Therefore, suitable production techniques are needed to produce supercapacitor electrode materials with ideal geometric shapes, appropriate charge transport behavior, controlled thickness, and surface chemical properties [122–125]. ALD, with its unique processing advantages, has become the primary technology for developing advanced generation supercapacitor electrode materials with superior macroscopic/nanoscale structures and surface properties [126–130]. The advantages of ALD, such as superior thickness control of the deposition layer, uniform deposition on large surface areas, consistency in deposition on complex features, and ease of manufacturing composite nanostructures, make it particularly suitable for application in energy storage devices [131–134].

4.1.1. ALD for Thin Film Electrode Materials

The uniform thickness of thin film electrode materials for supercapacitors is crucial for achieving rapid electrochemical response, as it helps to shorten the diffusion length of charges and ions [135,136]. In addition, thin film electrode materials directly affect the performance of supercapacitors, including energy density, power density, cycle stability, and charge and discharge rates [137]. Thin film electrodes have a thin and uniform thickness, which not only ensures rapid electrochemical response during charging and discharging processes, but also allows for the use of thin film electrodes in portable and/or miniaturized devices [138]. The research on thin film electrode materials includes the optimization of the mechanical strength and electrochemical properties of the materials. For example, by combining two-dimensional materials such as MXenes with one-dimensional materials such as nanocellulose, researchers have developed supercapacitor electrode materials with both high mechanical strength and excellent electrochemical performance. This hybrid material not only maintains high conductivity but also exhibits excellent mechanical strength, allowing supercapacitors to bend and roll without sacrificing performance [139].

ALD technology possesses a suite of significant advantages in the fabrication of thin-film electrode materials, rendering it an essential tool in the development of energy storage devices such as supercapacitors. Through precise control of chemical reactions, ALD enables the layer-by-layer deposition of films on material surfaces, achieving atomic-level control over film growth. This technique can introduce ultra-thin and uniform coatings on material surfaces, effectively enhancing interfacial compatibility and improving performance and safety [140–142]. Lopa et al. utilized ALD technology to fabricate WO_3 - MoO_3 nanocomposite electrodes with a thickness of less than 10.0 nm for supercapacitor applications, as depicted in Figure 8a–c. The thickness of the WO_3 and MoO_3 layers exhibited a good linear relationship with the number of ALD cycles, demonstrating the precise control of film thickness in thin-film electrode materials achievable through ALD. The thickness of the WO_3 film deposited via ALD was approximately 3.95 nm, while that of the MoO_3 film was about 3.93 nm, as shown in Figure 8d–g. Through meticulous optimization and control, the prepared electrodes featured uniform thickness, high purity, and good interfacial contact. The fabricated heterostructure electrodes displayed excellent pseudocapacitive behavior, highlighting their suitability for energy storage applications (Figure 8h,i). At a high current density of 19.23 A g^{-1} , the specific capacitance (Cs) reached a value of 803.10 F g^{-1} . Furthermore, the electrode exhibited excellent cyclic stability and low Cs loss after 5000 GCD cycles, indicating its superior durability and long-term reliability for various applications. Additionally, they reported the fabrication of different film electrode materials for supercapacitors using ALD technology. The prepared SnO_2 - ZnO (Figure 8j–m) and SnO_2 - In_2O_3 (Figure 8n–p) thin-film electrode materials, with their uniform thickness,

high purity, and good crystallinity, demonstrated the versatility of ALD in depositing uniform thin-film electrode materials for supercapacitors. The excellent performance in long-term cyclic testing further confirmed the electrochemical stability of ALD-deposited thin-film electrode materials [143–145].

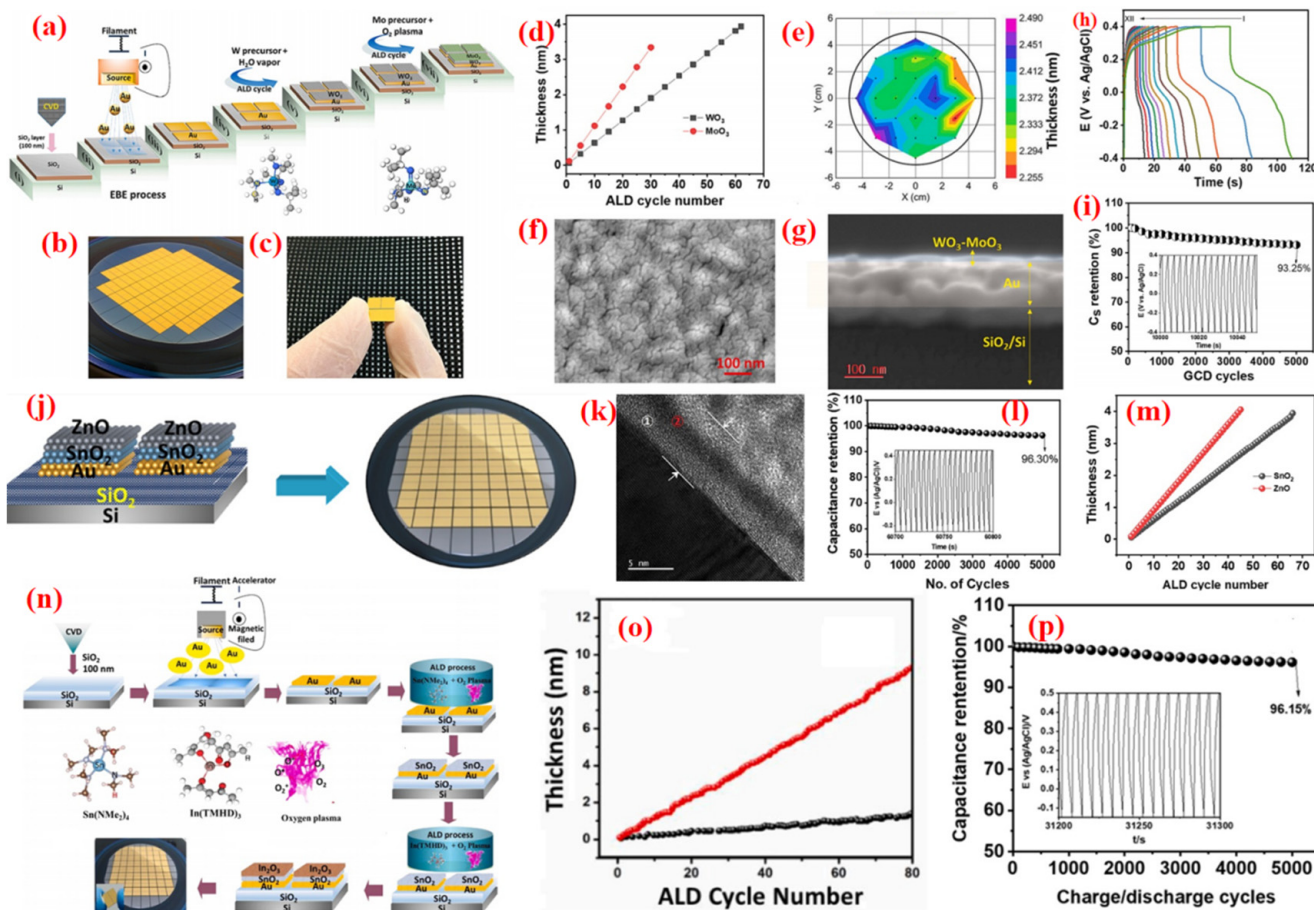


Figure 8. (a–c) Schematic representation of the fabrication steps involved in the production of WO_3 - MoO_3 electrodes; (d) thickness vs. ALD cycle number; (e) wafer scale spectroscopic ellipsometry measurements; (f) to-view and (g) cross-sectional FE-SEM images of the WO_3 - MoO_3 film; (h,i) electrochemical characterization. Reproduced with permission. Copyright 2024, Elsevier Publishing [143]. (j) Schematic illustration of 2D SnO_2 -ZnO heterojunction electrodes; (k) TEM images; (l) long-term cycle test of 2D SnO_2 -ZnO heterojunction electrodes; (m) film thickness vs. ALD cycle number monitored by an in situ sensing electrode for SnO_2 and ZnO. Reproduced with permission. Copyright 2023, ACS Publishing [144]. (n) Schematic illustration of 2D SnO_2 - In_2O_3 electrodes; (o) film thickness vs. ALD cycle number for SnO_2 and In_2O_3 ; (p) long-term cycle test. Reproduced with permission. Copyright 2022, Elsevier Publishing [145].

4.1.2. ALD for Surface Coating of Electrode Materials

The application of coating layers in supercapacitor electrode materials plays a multi-faceted role in enhancing the performance and stability of the electrodes. Coating layers provide a protective barrier for electrode materials, which reduces side reactions between active substances and the electrolyte, thereby extending the cycle life of the supercapacitor [146,147]. Coating layers also improve the interfacial compatibility of electrode materials, facilitating the transport of electrons and ions. In some cases, coating layers can act as a medium to increase the specific surface area of electrode materials, offering more charge storage sites [148]. The optimization of structure helps to increase the power density and energy density of supercapacitors [149,150]. Furthermore, coating layers enhance

the structural stability of electrode materials, particularly during volume expansion or contraction in the charging and discharging processes. This protective effect is conducive to maintaining the integrity of the electrode materials, reducing structural degradation, and thus improving the long-term stability and reliability of supercapacitors [151,152].

ALD plays a significant role in the construction of coating layers for supercapacitor electrode materials. ALD enables precise control over chemical reactions, allowing for the layer-by-layer deposition of thin films on material surfaces and achieving atomic-level thin-film growth. This effectively enhances the material's interfacial compatibility [153]. Films deposited by ALD, such as aluminum oxide, exhibit excellent thermal stability. Electrodes coated with these films can maintain better performance when operating at high temperatures, reducing the risk of thermal runaway [154], further enhancing the performance and safety of supercapacitors. Adhikari et al. successfully constructed freestanding core–shell NiO/Co₃O₄ electrodes on nickel foam by growing cobalt nancone structures through a simple hydrothermal method, followed by annealing to form Co₃O₄. The advanced atomic layer deposition (ALD) technique was then employed to produce a shell of NiO on the Co₃O₄ nancone structures. The Co₃O₄ structure serves as a layered substrate for the NiO atoms and conforms to the shape of the substrate, forming a core–shell structure. The layer-by-layer precipitation simplifies the process for controlling the thickness and uniformity of the Co₃O₄@NF. The deposited NiO adopts the primary nanoparticle shape with a nancone structure. The optimized NiO/Co₃O₄@NF exhibits a specific capacitance of 1242 C g⁻¹ (2760 F g⁻¹) at a current density of 2 A g⁻¹ and retains a capacitance of 959.8 C g⁻¹ (2133 F g⁻¹) at a current density of 10 A g⁻¹, demonstrating superior electrochemical performance. After 12,000 charge–discharge cycles, the material's capacitance retention is about 95.5%, which is exceptionally high compared with the retention capability of Co₃O₄@NF. Impedance studies confirm that the NiO/Co₃O₄@NF nancone structure has low charge transfer resistance, and the better interaction between the core and shell facilitates faster transport phenomena. The excellent electrochemical performance of NiO/Co₃O₄@NF is not only attributed to the synergistic effect of the core Co₃O₄ and the atomic layer-deposited NiO shell but also to the effective stabilization of the Co₃O₄ structure against degradation by the ALD NiO protective shell, while maintaining superior electrochemical properties [155].

In addition to stabilizing the structure, ALD coatings play a significant role in enhancing electrochemical performance by increasing the specific surface area of electrode materials and the electronic synergy between layers. For instance, Pawar et al. reported the excellent performance of hierarchical nanosheets modified with an ultrathin molybdenum disulfide (MoS₂) layer on NiCo₂O₄ electrodes for supercapacitor applications. As shown in Figure 9a, an ultrathin MoS₂ layer was synthesized on the NiCo₂O₄ surface using the atomic layer deposition (ALD) method. From the TSEM images shown in Figure 9b,c, the NiCo₂O₄ nanosheets are much thinner than the Co₃O₄ hexagonal nanosheets, which may positively impact achieving a larger surface area and more active sites, conducive to higher capacitance values. At the same time, the ALD-MoS₂ layer has a rough surface at the atomic scale, which also increases the total surface area of the electrode, significantly improving the charge storage capacitance [156,157]. The thinner and well-connected NiCo₂O₄ nanosheets provide more interfaces between the electrode and electrolyte, while the optimal thickness of MoS₂ contributes to maximizing device performance. According to CV measurements, shown in Figure 9d, a significant portion of the capacitance is transmitted through Faradaic reactions. The high surface capacitance (2445 mF cm²) and enhanced rate performance of the optimized NiCo₂O₄-MoS₂ composite material are attributed to the synergistic effects of the high specific surface area of the oxide nanosheets and the better electronic conductivity of the sulfide (Figure 9e–g) [158].

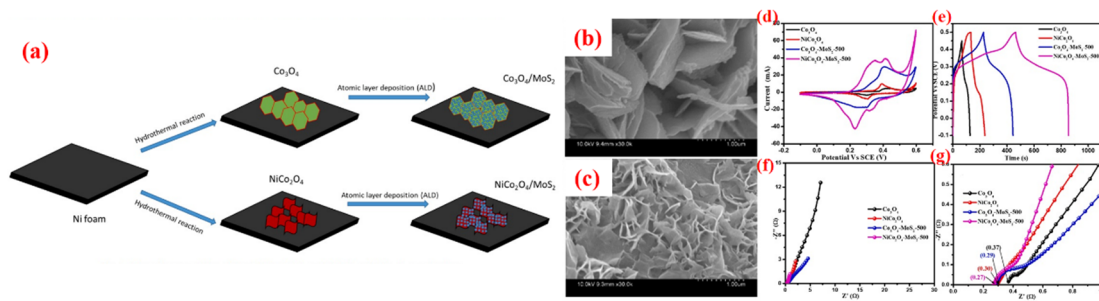


Figure 9. (a) Schematic representation of the synthesis of MoS₂-coated Co₃O₄ and NiCo₂O₄ nanosstructures; (b,c) FESEM images of Co₃O₄-MoS₂ and NiCo₂O₄-MoS₂; (d–g) electrochemical behaviors of NiCo₂O₄-MoS₂. Reproduced with permission. Copyright 2022, Elsevier Publishing [158].

4.1.3. ALD for Loaded Nanoparticle

The application of nanoparticles in the electrode materials of supercapacitors has significantly enhanced their electrochemical performance. These nanoparticles can serve as dopants to modify the surface of electrode materials or embed in composite materials to effectively reduce resistance and increase specific capacitance [159–161]. For instance, low-crystallinity iron oxyhydroxide nanoparticles, as anode materials for supercapacitors, have demonstrated excellent electrochemical energy storage characteristics. Their design and assembly in aqueous electrolytes can yield supercapacitor energy storage devices with high energy density, high power density, and long cycle life [162]. Nanoparticles can be directly used as electrode materials, and although they are susceptible to oxidation, their stability and performance can be significantly improved through appropriate protective layers or by compounding with other materials. Metal nanoparticles can even act as current collectors, especially precious metals like gold or platinum, due to their excellent stability and high conductivity [163,164]. Furthermore, the introduction of nanoparticles can increase the specific surface area of electrode materials, thereby providing more charge storage sites [165].

As depicted in Figure 10a, Hai et al. employed the ALD method to deposit WO₃ and TiO₂ on a SiO₂/Si substrate, with a subsequent annealing process leading to the aggregation of TiO₂ films into nanoparticles, thereby functionalizing the WO₃ electrode material with TiO₂ nanoparticles. It is clearly observable from Figure 10b–d that the top blank electrode exhibits a bright yellow color, while both the two-dimensional WO₃ electrode on the left and the two-dimensional TiO₂NP-WO₃ electrode on the right display a deep yellow, indicating the deposition of WO₃ and TiO₂NP-WO₃ nanofilms. In contrast to the pure two-dimensional WO₃ film (Figure 10e), TiO₂ after annealing is uniformly distributed on the WO₃ surface in the form of small nanoparticles, with the ultrathin TiO₂ layer gradually condensing into small nanoparticles in air at 380 °C (Figure 10f,g), resulting in an increased surface area. The GCD test results reveal that the surface functionalization of the two-dimensional WO₃ electrode with TiO₂ nanoparticles shifts the capacitive behavior from double-layer capacitance to pseudocapacitance, with a significant increase in specific capacitance of approximately 1.5 times (Figure 10h,i). CV and rate capability tests also demonstrate the enhanced electrochemical performance of the 2D TiO₂NP-WO₃ electrode (Figure 10j,k) [166].

In summary, atomic layer deposition (ALD) technology exhibits notable advantages in the preparation of electrode materials for supercapacitors. The high precision and uniformity ensure the superior performance of electrode materials, with the capability of achieving monolayer deposition that ensures uniform coverage even on complex shapes and structures. Table 1 compares the electrochemical performance of supercapacitor electrodes prepared by ALD with those prepared by other methods. It can be observed that the electrochemical performance of the electrodes deposited via ALD is significantly higher than that of electrodes synthesized by other techniques. ALD technology holds broad appli-

cation prospects and significant research value in the field of electrode material preparation for supercapacitors.

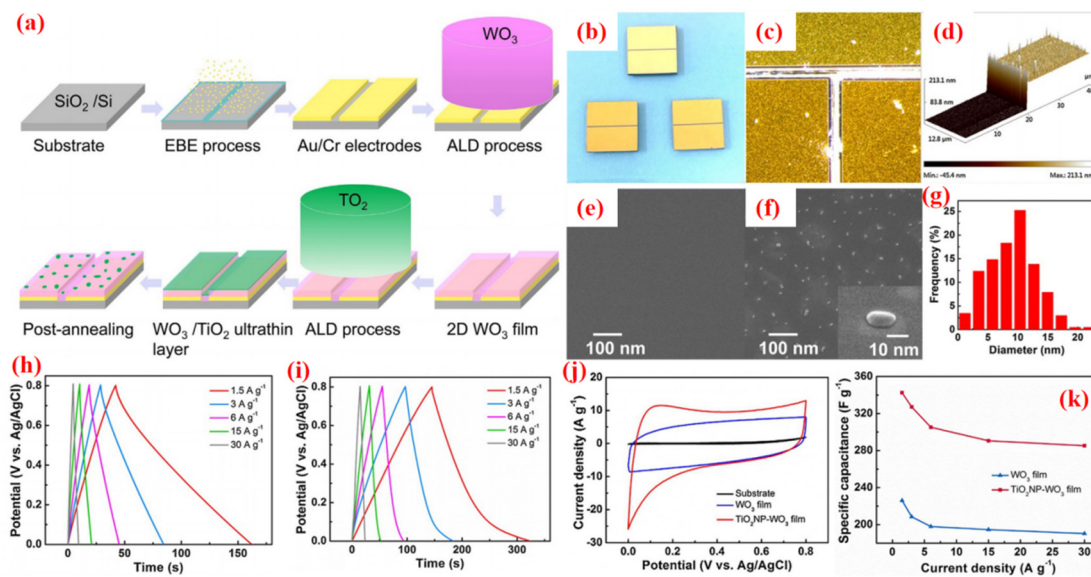


Figure 10. (a) Schematic illustration of TiO₂NP-WO₃ film; (b) optical image of the samples; (c) high-resolution optical image of the samples; (d) AFM image; (e) 2D WO₃ film and (f) 2D TiO₂NP-WO₃ film after post-annealing; (g) size distribution histogram of TiO₂ nanoparticles; (h–k) electrochemical behaviors. Reproduced with permission. Copyright 2017, Elsevier Publishing [166].

Table 1. Summary of electrochemical performance of ALD-based electrodes in comparison to other preparation methods.

Electrodes Prepared via ALD	Electrochemical Performance	Electrodes Prepared by Other Methods	Electrochemical Performance	Ref.
MoS ₂	$C_{sp} = 3400 \text{ mF cm}^{-2}$ at 3 mA cm ⁻² , $C_R = 82\%$ after 4000 cycles	MoS ₂	$C_{sp} = 403 \text{ F g}^{-1}$ at 1 mV s ⁻¹ , $C = 80\%$ after 2000 cycles at 150 mV s ⁻¹	[167–169]
Co ₉ S ₈	$C_{sp} = 1309 \text{ F g}^{-1}$ at 45 A g ⁻¹ , $C_R = 94.4\%$ after 2000 cycles at 45 A g ⁻¹	MoS ₂ quantum sheets	$C_{sp} = 140 \text{ F g}^{-1}$ at 5 mV s ⁻¹ , $C_R = 84\%$ after 5000 cycles at 7.5 mA s ⁻¹	[170–172]
TiO ₂	$C_{sp} = 2332 \text{ F g}^{-1}$ at 1 A g ⁻¹	Co ₉ S ₈ /CNF	$C_{sp} = 718 \text{ F g}^{-1}$ at 1 A g ⁻¹ , $C_R = 83.1\%$ after 5000 cycles at 10 A g ⁻¹	[173–175]
V ₂ O ₅	$C_{sp} = 540 \text{ F g}^{-1}$, $C_R = 89\%$ after 10,000 cycles at 5 A g ⁻¹	Co ₉ S ₈ @C	$C_{sp} = 514 \text{ F g}^{-1}$ at 1 A g ⁻¹ , $C_R = 88\%$ after 1000 cycles at 8 A g ⁻¹	
		TiO ₂ -rGO	$C_{sp} = 338 \text{ F g}^{-1}$ at 5 mV s ⁻¹ , $C_R = 93.3\%$ after 3000 cycles at 2.5 A g ⁻¹	
		TiO ₂ -NF	$C_{sp} = 1052 \text{ F g}^{-1}$ at 25 mV s ⁻¹ , $C_R = 80\%$ after 5000 cycles at 7 A g ⁻¹	
		V ₂ O ₅	$C_{sp} = 204 \text{ C g}^{-1}$ at 1 A g ⁻¹	[176–178]
		V ₂ O ₅	$C_{sp} = 437 \text{ F g}^{-1}$ at 1 A g ⁻¹ , $C_R = 91\%$ after 10,000 cycles	

Table 1. Cont.

Electrodes Prepared via ALD	Electrochemical Performance	Electrodes Prepared by Other Methods	Electrochemical Performance	Ref.
RuO ₂	$C_{sp} = 644 \text{ F g}^{-1}$, $C_R = 117\%$ after 2000 cycles	RuO ₂ /PCs	$C_{sp} = 539.6 \text{ F g}^{-1}$ at 5 mV s ⁻¹ , $C_R = 98\%$ after 1000 cycles at 5 A g ⁻¹	[179–181]
		RuO ₂	$C_{sp} = 209 \text{ F g}^{-1}$ at 45 A g ⁻¹ , $C_R = 94.4\%$ after 2000 cycles at 45 A g ⁻¹	
NiO/CNC	$C_{sp} = 430 \text{ C g}^{-1}$ at 1 A g ⁻¹ , $C_R = 95.5\%$ after 12,000 cycles at 5 A g ⁻¹	C/NiO	$C_{sp} = 585 \text{ F g}^{-1}$ at 1 A g ⁻¹ , $C_R = 100\%$ after 6000 cycles at 5 A g ⁻¹	[182–184]
		NiO/rGO	$C_{sp} = 435.25 \text{ F g}^{-1}$ at 1 A g ⁻¹	
	$C_{sp} = 2760 \text{ F g}^{-1}$ at 2 A g ⁻¹ , $C_R = 95.5\%$ after 12,000 cycles at 5 A g ⁻¹	NiO/Co ₃ O ₄	$C_{sp} = 405 \text{ F g}^{-1}$ at 1 A g ⁻¹ , $C_R = 97.4\%$ after 1000 cycles at 15 A g ⁻¹	[155,185,186]
Ni ₃ C/CNT	$C_{sp} = 1850 \text{ F g}^{-1}$ at 2 mA cm ⁻² , $C_R = 98.5\%$ after 5000 cycles at 20 mA cm ⁻²	NiO/Co ₃ O ₄	$C_{sp} = 1303.9 \text{ F g}^{-1}$ at 1 A g ⁻¹ , $C_R = 88.5\%$ after 10,000 cycles at 10 A g ⁻¹	
		g-C ₃ N ₄ /Ni ₃ C	$C_{sp} = 1137.3 \text{ F g}^{-1}$ at 1 A g ⁻¹	[187–189]
		Ni ₃ C	$C_{sp} = 390 \text{ C g}^{-1}$ at 0.5 A g ⁻¹ , $C_R = 86.9\%$ after 3000 cycles at 2 A g ⁻¹	
NiCo ₂ O ₄ /NiO	$C_{sp} = 2439 \text{ F g}^{-1}$ at 45 A g ⁻¹ , $C_R = 94.2\%$ after 20,000 cycles at 4 A g ⁻¹	NiO/NiCo ₂ O ₄	$C_{sp} = 866 \text{ F g}^{-1}$ at 5 mV s ⁻¹ , $C_R = 85\%$ after 5000 cycles at 5 A g ⁻¹	[129,190,191]
		NiO/NiCo ₂ O ₄	$C_{sp} = 1623 \text{ F g}^{-1}$ at 2 A g ⁻¹ , $C_R = 90\%$ after 10,000 cycles at 10 A g ⁻¹	

4.2. Defect Engineering via ALD for Supercapacitors

In the previous content, the role of ALD in defect engineering and electrode material preparation for supercapacitors was reviewed. The application of defect engineering in supercapacitors through ALD is a promising technical strategy. By precisely controlling the types and distribution of defects in electrode materials, the electrochemical performance of supercapacitors can be significantly improved.

4.2.1. Oxygen Vacancies

Oxygen vacancies play a pivotal role in supercapacitors, enhancing the electrochemical performance of electrode materials through multifaceted mechanisms. The introduction of oxygen vacancies can increase the number of active sites on the surface of electrode materials, thereby improving the charge transfer efficiency between the electrode and the electrolyte [192,193]. Additionally, the incorporation of oxygen vacancies can enhance electronic transport properties, reduce charge transfer resistance, and result in a faster kinetic response of the electrode material during charging and discharging processes [194,195]. The regulatory effect of oxygen vacancies can also optimize the surface properties of electrode materials, such as hydrophilicity and electrochemical stability, thereby enhancing the wettability and long-term stability of the materials in the electrolyte [196,197]. The microstructure of the material can be further optimized through the introduction of oxygen vacancies, such as pore size distribution and specific surface area, providing more stor-

age space for electrolyte ions and consequently increasing the specific capacitance of the electrode material [198,199]. Moreover, oxygen vacancies can promote pseudocapacitive behavior, enhancing the energy storage performance of supercapacitors through surface adsorption and redox reactions [200,201]. For instance, Wang et al. introduced a dual-defect strategy to synthesize Mo-doped NiCo_2O_4 (R-Mo-NiCo₂O₄) with abundant oxygen vacancies. By employing NaBH₄ reduction, oxygen vacancy defects were generated within the NiCo₂O₄ lattice, resulting in an increased carrier concentration and a substantially enhanced conductivity. This, in turn, facilitated the involvement of more active materials in electrochemical redox reactions, resulting in its significantly enhanced specific capacity, capacity retention, and cycling stability [202]. Additionally, Wang et al. modeled the bulk oxygen substitution and surface oxygen vacancies in ZnCo₂O₄ nanowires (F-ZnCo₂O_{4-x}) grown on nickel foam. The increase in oxygen vacancy concentration enhances the conductivity and electrochemical activity of the electrode. The surface O vacancies could lower the conduction band, serving as active sites for electron trapping. Therefore, the obtained F-ZnCo₂O_{4-x} electrode achieves a high specific capacity of 664 $\text{mAh}\cdot\text{g}^{-1}$ at 1 $\text{A}\cdot\text{g}^{-1}$ [203].

ALD can directly obtain supercapacitor electrode materials with oxygen vacancies. Kao et al. utilized atomic layer deposition (ALD) to deposit a conformal coating of titanium nitride (TiN) on the surface of a carbon nanotube forest. The increased surface oxygen vacancies in titanium nitride (TiN) facilitated Faradaic redox surface reactions, as depicted in Figure 11a,b. Figure 11c,d reveal the SEM images of a vertically aligned carbon nanotube forest coated with ALD TiN, where a forest approximately 30 μm in height was successfully grown. From the TEM images in Figure 11e,f, the exposed carbon nanotubes exhibit a hollow core and a multi-walled structure with a uniform coating thickness. The thickness of the TiN coating, corresponding to 400 ALD cycles, is approximately 20 nm, demonstrating a good uniformity. XPS measurements (Figure 11g) indicate a relatively high oxygen content on the electrode surface, suggesting a high concentration of oxygen in the native oxide layer. Furthermore, nitrogen doping in titanium dioxide materials has been shown to increase oxygen vacancies, thereby enhancing the potential for charge insertion and storage [204]. The capability to store more charge stems from the recombination of electrons associated with oxygen deficiency. Chemical testing (Figure 11h–j) demonstrates that the capacitance of the TiN-CNT devices increased by over 500% compared with bare carbon nanotubes (TiN-CNT at 81 mF/cm^2 , CNT electrode at 14 mF/cm^2), while the capacitance of the bare carbon nanotubes was nearly 400 times higher than that of the planar TiN electrode ($0.2 \text{ mF}/\text{cm}^2$) [80].

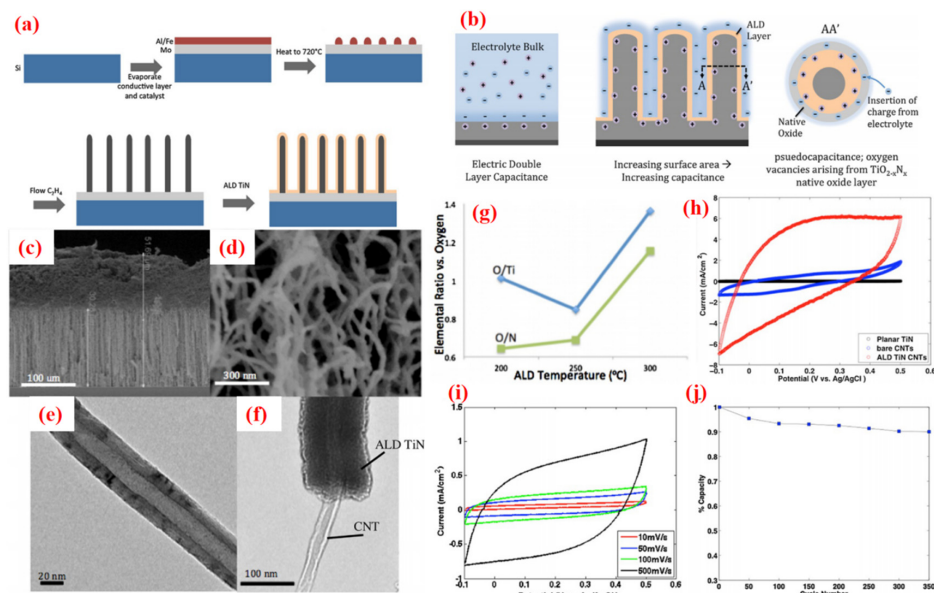


Figure 11. (a) Schematic presentation for TiN-CNT architecture; (b) conceptual illustration of increasing capacitance through increased surface area and the pseudo capacitive effect; (c) SEM image of

uncycled ALD TiN coated onto vertically aligned CNT forest; (d) close-up SEM image of uncycled ALD TiN-coated CNTs; (e) TEM image of single multiwalled carbon nanotube; (f) TEM image of ALD TiN-coated multiwalled carbon nanotube; (g) XPS characterization of ALD TiN; (h–j) electrochemical behaviors of ALD TiN-CNTs. Reproduced with permission. Copyright 2016, Elsevier Publishing [80].

4.2.2. Interface Defects

Interface defects play a critical role in supercapacitors, significantly enhancing the electrochemical performance of electrode materials through various mechanisms. The introduction of interface defects can increase the number of active sites on the surface of electrode materials, thereby improving the charge transfer efficiency between the electrode and the electrolyte [205,206]. Additionally, the integration of interface defects can enhance electron transport properties, reduce charge transfer resistance, and enable a faster dynamic response of the electrode material during charging and discharging processes [207,208]. The regulatory effect of interface defects can also optimize the surface properties of electrode materials, such as hydrophilicity and electrochemical stability, thereby modifying the material's wettability and long-term stability in the electrolyte [209,210]. Furthermore, interface defects can promote pseudocapacitive behavior, enhancing the energy storage performance of supercapacitors through surface adsorption and redox reactions [211,212]. For instance, Zhou et al. fabricated dual-transition metal oxide heterojunction (V_o -ZnO/CoO) nanowires with oxygen vacancies through hydrothermal and thermal treatments. The formation of the heterojunction led to the redistribution of interfacial charges between ZnO and CoO, generating an internal electric field that accelerated electron transfer. Due to the abundant electron density on the surface and unimpeded electron transfer within the bulk, the ZnO/CoO electrode exhibited higher capacity and superior cycling stability [213].

In addition to directly preparing electrode materials containing oxygen vacancies, oxygen vacancies can also be formed at the interface of multi-layer materials deposited by ALD. Zhang et al. employed plasma treatment and ALD technology to fabricate Al_2O_3 ALD coatings on activated carbon (AC) electrodes (Figure 12a). As shown in Figure 12b–e, the surface structure of the AC gradually became destroyed and roughened with the extension of plasma treatment time compared with the bare AC. Clearly, the AC structure could no longer maintain an intact block structure after 30 min. This may be attributed to the breakdown of original C-C bonds under the action of plasma energy, leading to the formation of new functional group bonds and defect structures. With the prolongation of processing time, the graphitization degree of the samples (named as OP- x , $x = 5, 15$ and 30) decreased, indicating that the introduction of oxygen led to an increase of defects. The ID/IG ratio of the four samples slightly increased with the extension of treatment time, indicating an increase in defects (Figure 12f). Impedance test results (Figure 12g) showed that the charge transfer resistances (R_{ct}) for the bare AC, OP-5, OP-15, and OP-30 were 17.5, 6.72, 6.62, and 6.98, respectively. The equivalent series resistance R_s values were 1.5, 0.945, 0.851, and 0.825, respectively; the induced oxygen doping led to more defects and a richer array of ion adsorption active sites. Additional oxygen was introduced into the AC electrodes through plasma treatment to increase the active sites and defects. This plasma-induced oxygen doping reduced the charge transfer resistance, improved the kinetics, and was beneficial for enhancing the capacitance and ion transport. It also resulted in superior electrochemical performance (Figure 12h,i). Moreover, The ALD coating layer can be observed more clearly from the TEM images, shown in Figure 12j–m. Compared with the exposed AC and OP-15 electrodes (Figure 12j,k), a roughly 2 nm thick Al_2O_3 layer can be detected on the carbon surface, as shown in Figure 12l,m. After 5000 retention test cycles, four battery samples were dissected to further inspect the degradation. The relatively intact thin layer maintained good stability, demonstrating the highly stability of the ALD-deposited film [214].

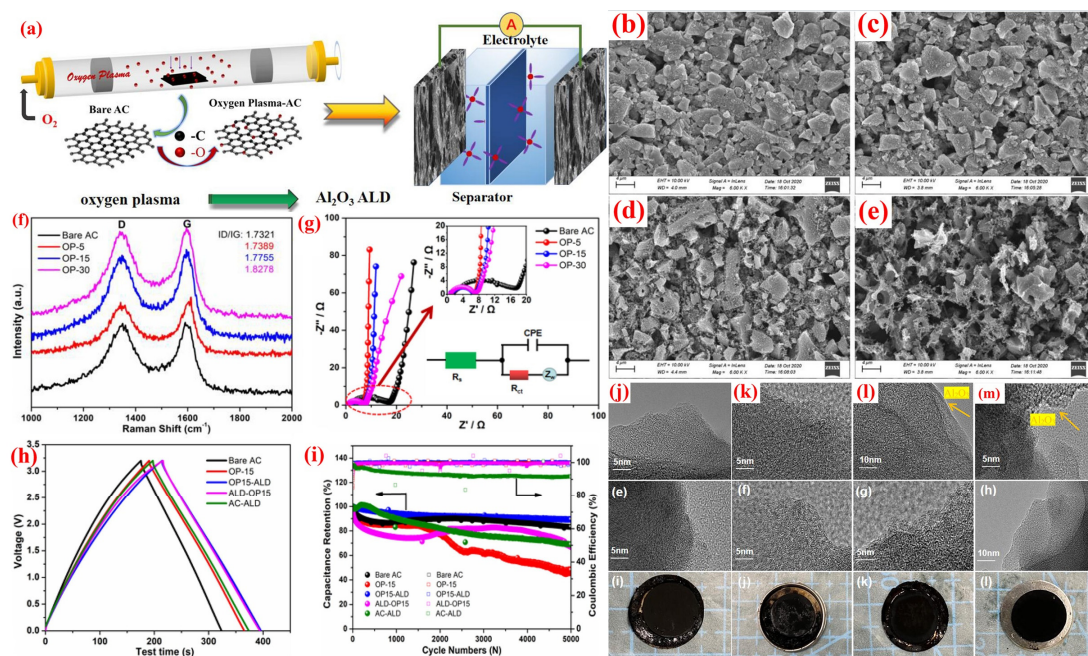


Figure 12. (a) Illustration for the function of oxygen plasma and Al_2O_3 ALD coating on the AC electrode. SEM image: (b) bare AC; (c) oxygen-plasma treatment at 5 min (OP-5); (d) oxygen-plasma treatment at 15 min (OP-15); (e) oxygen-plasma treatment at 30 min (OP-30). (f) Raman spectra; (g–i) Electrochemical behaviors. TEM image of fresh electrode: (j) bare AC; (k) OP-15; (l) ALD-OP15; (m) OP15-ALD. Reproduced with permission. Copyright 2024, Frontiers Publishing [214].

4.2.3. Passivation of Defects

Passivation of defect can significantly enhance electrochemical performance and stability of supercapacitors through the reduction of defects within electrode materials, such as vacancies, interstitials, and grain boundaries [215–217]. Defects act as traps for charge carriers, leading to hindered charge transport and consequently decreased capacitance and power density of the electrode materials [218,219]. Passivation techniques, including surface modification, doping, atomic layer deposition (ALD), and plasma treatment, can effectively fill these defects, thereby reducing charge transport resistance and improving the specific capacitance and cycling stability of electrode materials [220,221].

Graphene is considered an exciting electrode material for supercapacitors due to its excellent conductivity and large specific surface area [222–226]. However, the inherent defects in the oxidized/reduced graphene oxide structure reduce its conductivity and electrochemical performance, limiting its application in its original form. ALD provides a unique convenience for accurately functionalizing graphene oxide/reducing graphene oxide defects [227,228]. Yang et al. reported an optimization method for electrode materials utilizing a combined system of RuO_2 nanomaterials and graphene oxide. Initially, graphene oxide sheets were immobilized on carbon cloth via an electrochemical process. Subsequently, RuO_2 nanoparticles were grown on the immobilized graphene oxide using ALD with $\text{Ru}(\text{EtCp})_2$ [bis(ethylcyclopentadienyl)ruthenium] and O_2 as precursors (Figure 13a). As the number of deposition cycles increased, the size of the RuO_2 nanoparticles also enlarged (Figure 13b). The ALD precursors require a functional site for chemisorption during the first half of the reaction. Functional sites typically exist at defects. SEM and STEM images in Figure 13c–h revealed that individual carbon fibers were fully covered with graphene oxide sheets containing one or more graphene layers. This process tightly bound the graphene oxide to the carbon fibers. After undergoing the ALD step, randomly distributed RuO_2 nanoparticles were observed to grow on the reduced graphene oxide (rGO). As shown in Figure 13i–l, the synthesized composite exhibited a specific capacitance of 1132 F g^{-1} at a scan rate of 50 mV s^{-1} , approaching the theoretical limit. Traditional

two-electrode configurations indicated that the specific capacitance of the graphene oxide electrode increased by approximately 40% when the optimal Ru loading was about 9.3 wt%. RuO₂ selectively chemically bound to defect sites on the graphene oxide substrate, where C-O sites were initially replaced by C-O-Ru bonds, altering the chemical nature of these defects and exhibiting excellent electrochemical performance [229].

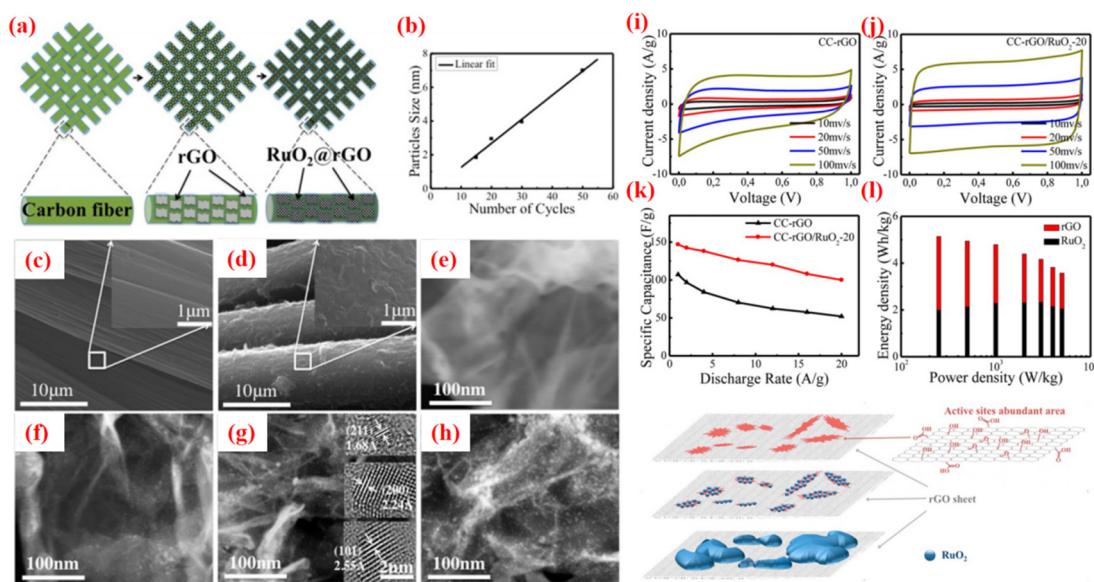


Figure 13. (a) Schematic of fabrication process of rGO/RuO₂; (b) average size dependence of RuO₂ nanoparticles on number of ALD cycles; (c,d) SEM images of (c) carbon fiber and (d) carbon fiber covered with rGO; (e–h) STEM images of (e) rGO, (f) rGO/RuO₂-15, (g) rGO/RuO₂-20, and (h) rGO/RuO₂-30; (i–l) electrochemical behaviors. Reproduced with permission. Copyright 2015, ACS Publishing [229].

5. Conclusions

This article provides an overview of ALD application in supercapacitors. It can be divided into several parts: ALD for defect engineering, ALD for the preparation of supercapacitor electrode materials, and defect engineering of electrode materials through ALD. The summary is as follows:

- (1) ALD technology is effective in defect engineering, allowing for the direct deposition of thin films by adjusting deposition parameters or introducing defects at the interfaces between film layers through controlled deposition sequences and cycles. In terms of defect passivation, ALD can precisely fill and cover defects to enhance the stability of materials, influencing the electrical, optical, and mechanical properties of nanomaterials, optoelectronic devices, and catalysts.
- (2) ALD technology enables precise control over the composition and structure of electrode materials, directly impacting their electrochemical performance in supercapacitors. By selecting appropriate precursors and deposition conditions, ALD can not only directly fabricate thin-film electrodes with excellent electrochemical properties for supercapacitors but also increase the specific surface area and stability of electrode materials through the deposition of covering layers, while optimizing these conditions further refines the morphology and structure of the thin films.
- (3) ALD technology is also a potential tool for defect engineering, significantly enhancing the electrochemical performance of supercapacitor electrode materials. Electrode materials prepared containing oxygen vacancies through ALD can promote Faradaic oxidation-reduction surface reactions, enhancing the ability of electrodes to store electrical charge. The formation of interface defects using ALD can enhance electron transport performance and reduce charge transfer resistance, as well as make the

dynamic response of electrode materials faster during charging and discharging processes. Furthermore, with the advantage of atomic-level control, ALD can precisely repair defects on the surface of electrode materials, improving inherent electrical conductivity, thus enhancing electrochemical performance.

In addition, there are also some challenges in applying defect engineering via ALD for supercapacitors.

- (1) ALD demonstrates significant potential in the fabrication of supercapacitor electrode materials, with unique advantages including precise thickness control and excellent deposition quality, which play a crucial role in the field of energy storage, particularly in the construction and of supercapacitor electrode materials. ALD can optimize the electrochemical performance of electrode materials, such as specific surface area and conductivity, thereby enhancing the specific capacitance of supercapacitors and achieving high energy and power density. However, ALD technology also faces challenges in the preparation of supercapacitor electrode materials, including the complex charge storage issues of high-loading electrodes, performance requirements under unconventional/extreme conditions, and the understanding of the structure–property relationship. These challenges necessitate further research and exploration by scientific researchers to achieve the commercial application of supercapacitor electrode materials.
- (2) ALD with precise control over thickness and exceptional deposition quality offers unique advantages in the defect engineering for supercapacitor electrode materials. Through precisely controlling defects, including the type, quantity, and distribution, the electrochemical performance can be optimized, such as specific surface area and conductivity, thereby enhancing the energy density, power density, and cyclic stability of supercapacitors. However, implementing defect engineering requires precise control over deposition conditions, reaction mechanisms, and surface chemical processes, increasing the technical difficulty and complexity.
- (3) While atomic layer deposition (ALD) has demonstrated remarkable potential in a wide array of applications, transitioning this advanced technology from the laboratory to commercial-scale production presents a multitude of challenges. Among these, maintaining precise process control, ensuring material quality and uniformity across larger substrates, and managing the economic viability of ALD systems stand out as critical areas requiring further attention. Additionally, the scalability of ALD infrastructure to meet industrial demands, as well as the need for continuous innovation in materials and processes to address market trends and emerging applications, pose significant hurdles. As such, future research should focus on developing scalable and cost-effective ALD technologies, exploring new materials and deposition strategies, and optimizing process parameters to enhance productivity and material performance. Addressing these challenges will be instrumental in unlocking the full commercial potential of ALD, paving the way for its broader adoption and integration into industrial manufacturing processes.
- (4) ALD, besides demonstrating immense potential in the preparation of electrode materials for supercapacitors, also holds significant promise for other sustainable and scalable energy applications. However, it still faces numerous challenges. For instance, ALD technology can be employed to construct protective layers on lithium metal surfaces to suppress the growth of lithium dendrites. Yet, research is still required to ensure the stability and long-term effectiveness of these protective layers. In lithium-sulfur batteries, ALD technology can be utilized to build barrier layers on cathodes or separators to inhibit the shuttle of polysulfides. Nevertheless, further investigation is needed to guarantee the permeability and ionic conductivity of these barrier layers. In sodium-ion batteries, where sodium exhibits higher chemical reactivity than lithium, ALD coatings need to provide superior interface stability to prevent the decomposition of electrolytes.

Author Contributions: Writing—original draft preparation, T.G.; Conceptualization, X.X. and Z.D.; Writing—review and editing, X.L., L.M. and J.W.; Project administration, Y.L.; funding acquisition, Q.H. and J.X. All authors have read and agreed to the published version of the manuscript.

Funding: This work was supported by National Key R&D Program of China (Grant No. 2022YFC3320700), National Natural Science Foundation of China (Grant No. 22302118), Beijing Nova Program (20230484316) and China Postdoctoral Science Foundation (No. 2022M712019).

Data Availability Statement: All collected data are presented in the manuscript.

Conflicts of Interest: The authors declare no conflict of interest.

References

- Zong, W.; Lai, F.; He, G.; Feng, J.; Wang, W.; Lian, R.; Miao, Y.E.; Wang, G.C.; Parkin, I.P.; Liu, T. Sulfur-Deficient Bismuth Sulfide/Nitrogen-Doped Carbon Nanofibers as Advanced Free-Standing Electrode for Asymmetric Supercapacitors. *Small* **2018**, *14*, 1801562. [[CrossRef](#)] [[PubMed](#)]
- Zhong, C.; Deng, Y.; Hu, W.; Qiao, J.; Zhang, L.; Zhang, J. A review of electrolyte materials and compositions for electrochemical supercapacitors. *Chem. Soc. Rev.* **2015**, *44*, 7484–7539. [[CrossRef](#)] [[PubMed](#)]
- Zhang, Y.; Liu, L.; Zhang, L.; Yu, Y.; Lv, H.; Chen, A. Template-free method for fabricating carbon nanotube combined with thin N-doped porous carbon composite for supercapacitor. *J. Mater. Sci.* **2019**, *54*, 6451–6460. [[CrossRef](#)]
- Muzaffar, A.; Ahamed, M.B.; Hussain, C.M. Green supercapacitors: Latest developments and perspectives in the pursuit of sustainability. *Renew. Sustain. Energy Rev.* **2024**, *195*, 114324. [[CrossRef](#)]
- Padalkar, N.S.; Sadavar, S.V.; Shinde, R.B.; Patil, A.S.; Patil, U.M.; Dhawale, D.S.; Bulakhe, R.N.; Kim, H.; Im, H.; Vinu, A.; et al. Layer-by-layer nanohybrids of Ni-Cr-LDH intercalated with 0D polyoxotungstate for highly efficient hybrid supercapacitor. *J. Colloid Interface Sci.* **2022**, *616*, 548–559. [[CrossRef](#)]
- Cai, B.; Li, J.; Wang, L.; Li, X.; Yang, X.; Lü, W. Enhanced performance of asymmetric supercapacitor based on NiZn-LDH@NiCoSe₂ electrode materials. *Nanotechnology* **2022**, *33*, 295402. [[CrossRef](#)]
- Zhong, M.; Zhang, M.; Li, X. Carbon nanomaterials and their composites for supercapacitors. *Carbon Energy* **2022**, *4*, 950–985. [[CrossRef](#)]
- Xiong, Y.; Zhang, Y.-F.; Zhu, C.-L.; Yang, L.; Liang, H.-Y.; Shi, J.; Chen, J.-W.; Tian, W.-Q.; Liu, S.; Li, Z.; et al. Carbon cathode with heteroatom doping and ultrahigh surface area enabling enhanced capacitive behavior for potassium-ion hybrid capacitors. *Rare Met.* **2024**, *43*, 2136–2149. [[CrossRef](#)]
- Wang, L.; Zhang, X.; Kong, Y.-Y.; Li, C.; An, Y.-B.; Sun, X.-Z.; Wang, K.; Ma, Y.-W. Metal–organic framework-derived CoSe₂@N-doped carbon nanocubes for high-performance lithium-ion capacitors. *Rare Met.* **2024**, *43*, 2150–2160. [[CrossRef](#)]
- Shao, Y.; El-Kady, M.F.; Sun, J.; Li, Y.; Zhang, Q.; Zhu, M.; Wang, H.; Dunn, B.; Kaner, R.B. Design and Mechanisms of Asymmetric Supercapacitors. *Chem. Rev.* **2018**, *118*, 9233–9280. [[CrossRef](#)]
- Augustyn, V.; Simon, P.; Dunn, B. Pseudocapacitive oxide materials for high-rate electrochemical energy storage. *Energy Environ. Sci.* **2014**, *7*, 1597. [[CrossRef](#)]
- Tang, C.; Wang, X.; Ma, M.; Wang, Z.; Li, Y.; Li, H.; Li, B.; Zhang, Y.; Zhu, X. Optimizing the electrons/ions diffusion kinetics in δ-MnO₂ for realizing an ultra-high rate-capability supercapacitor. *Chem. Eng. J.* **2023**, *471*, 144784. [[CrossRef](#)]
- Song, Z.; Bi, R.; Li, J.; He, Y.; Rao, F.; Chen, X.; Wang, J.; Wang, Z.; Yu, R.; Wang, D. Metallic 1T-MoS₂ boosts the kinetics for NiS₂-based hybrid supercapacitors with superb rate performance. *J. Mater. Sci. Technol.* **2024**. [[CrossRef](#)]
- Shinde, P.A.; Olabi, A.G.; Chodankar, N.R.; Patil, S.J.; Hwang, S.-K.; Abdelkareem, M.A. Realizing superior redox kinetics of metal–metal carbides/carbon coordination supported heterointerface for stable solid-state hybrid supercapacitor. *Chem. Eng. J.* **2023**, *454*, 140246. [[CrossRef](#)]
- Thalji, M.R.; Ali, G.A.M.; Shim, J.-J.; Chong, K.F. Cobalt-doped tungsten suboxides for supercapacitor applications. *Chem. Eng. J.* **2023**, *473*, 140246. [[CrossRef](#)]
- Beknalkar, S.A.; Teli, A.M.; Satale, V.V.; Amate, R.U.; Morankar, P.J.; Yewale, M.A.; Shin, J.C. A critical review of recent advancements in high-temperature supercapacitors: Thermal kinetics, interfacial dynamics, employed strategies, and prospective trajectories. *Energy Storage Mater.* **2024**, *66*, 103217. [[CrossRef](#)]
- Malavekar, D.; Pujari, S.; Jang, S.; Bachankar, S.; Kim, J.H. Recent Development on Transition Metal Oxides-Based Core–Shell Structures for Boosted Energy Density Supercapacitors. *Small* **2024**, *20*, 202312179. [[CrossRef](#)]
- Pu, S.; Wang, Z.; Xie, Y.; Fan, J.; Xu, Z.; Wang, Y.; He, H.; Zhang, X.; Yang, W.; Zhang, H. Origin and Regulation of Self-Discharge in MXene Supercapacitors. *Adv. Funct. Mater.* **2022**, *33*, 202208715. [[CrossRef](#)]
- Lan, S.; Yu, C.; Yu, J.; Zhang, X.; Liu, Y.; Xie, Y.; Wang, J.; Qiu, J. Recent Advances in Low-Temperature Liquid Electrolyte for Supercapacitors. *Small* **2024**, 202309286. [[CrossRef](#)]
- Lyu, S.; Chang, H.; Zhang, L.; Wang, S.; Li, S.; Lu, Y.; Li, S. High specific surface area MXene/SWCNT/cellulose nanofiber aerogel film as an electrode for flexible supercapacitors. *Compos. Part B: Eng.* **2023**, *264*, 110888. [[CrossRef](#)]
- Wang, T.; Liu, Z.; Li, P.; Wei, H.; Wei, K.; Chen, X. Lignin-derived carbon aerogels with high surface area for supercapacitor applications. *Chem. Eng. J.* **2023**, *466*, 143118. [[CrossRef](#)]

22. Chen, S.; Xu, Q.; Chen, L.; Hu, Y.; Jiang, H.; Li, C. Engineering V₂O₃ nanoarrays with abundant localized defects towards high-voltage aqueous supercapacitors. *J. Mater. Chem. A* **2022**, *10*, 4825–4832. [[CrossRef](#)]
23. Ji, Z.; Tang, G.; Chen, L.; Zhong, J.; Chen, Y.; Zhu, G.; Chuan, X.; Zhang, J.; Shen, X. Defect engineering of hollow porous N, S co-doped carbon spheres-derived materials for high-performance hybrid supercapacitors. *Chem. Eng. J.* **2024**, *480*, 148213. [[CrossRef](#)]
24. Sun, Y.; Li, T.; Liu, X.; Han, Y.; Liu, Y.; Zada, A.; Deng, W.; Yuan, Z.; Dang, A. Modulating oxygen vacancies in MXene/MoO_{3-x} smart fiber by defect engineering for ultrahigh volumetric energy density supercapacitors and wearable SERS sensors. *Chem. Eng. J.* **2024**, *494*, 152911. [[CrossRef](#)]
25. Lu, W.; Yan, L.; Ye, W.; Ning, J.; Zhong, Y.; Hu, Y. Defect engineering of electrode materials towards superior reaction kinetics for high-performance supercapacitors. *J. Mater. Chem. A* **2022**, *10*, 15267–15296. [[CrossRef](#)]
26. Wang, Q.; Qu, Z.; Chen, S.; Zhang, D. Metal organic framework derived P-doping CoS@C with sulfide defect to boost high-performance asymmetric supercapacitors. *J. Colloid Interface Sci.* **2022**, *624*, 385–393. [[CrossRef](#)]
27. Peng, Z.; Li, S.; Huang, Y.; Guo, J.; Tan, L.; Chen, Y. Sodium-Intercalated Manganese Oxides for Achieving Ultra-Stable and Fast Charge Storage Kinetics in Wide-Voltage Aqueous Supercapacitors. *Adv. Funct. Mater.* **2022**, *32*, 202206539. [[CrossRef](#)]
28. Fu, Y.; Gao, X.; Zha, D.; Zhu, J.; Ouyang, X.; Wang, X. Yolk-shell-structured MnO₂ microspheres with oxygen vacancies for high-performance supercapacitors. *J. Mater. Chem. A* **2018**, *6*, 1601–1611. [[CrossRef](#)]
29. Yang, J.; Xiao, X.; Chen, P.; Zhu, K.; Cheng, K.; Ye, K.; Wang, G.; Cao, D.; Yan, J. Creating oxygen-vacancies in MoO₃- nanobelts toward high volumetric energy-density asymmetric supercapacitors with long lifespan. *Nano Energy* **2019**, *58*, 455–465. [[CrossRef](#)]
30. Li, G.; Cui, X.; Song, B.; Ouyang, H.; Wang, K.; Sun, Y.; Wang, Y. One-pot synthesis of Cu-doped Ni₃S₂ nano-sheet/rod nanoarray for high performance supercapacitors. *Chem. Eng. J.* **2020**, *388*, 124319. [[CrossRef](#)]
31. Ziegler, M.; Dathe, A.; Pollok, K.; Langenhorst, F.; Hübner, U.; Wang, D.; Schaaf, P. Metastable Atomic Layer Deposition: 3D Self-Assembly toward Ultradark Materials. *ACS Nano* **2020**, *14*, 15023–15031. [[CrossRef](#)] [[PubMed](#)]
32. Olowoyo, J.O.; Gharahshiran, V.S.; Zeng, Y.; Zhao, Y.; Zheng, Y. Atomic/molecular layer deposition strategies for enhanced CO₂ capture, utilisation and storage materials. *Chem. Soc. Rev.* **2024**, *53*, 5428–5488. [[CrossRef](#)] [[PubMed](#)]
33. Hui, L.; Nixon, R.; Tolman, N.; Mukai, J.; Bai, R.; Wang, R.; Liu, H. Area-Selective Atomic Layer Deposition of Metal Oxides on DNA Nanostructures and Its Applications. *ACS Nano* **2020**, *14*, 13047–13055. [[CrossRef](#)] [[PubMed](#)]
34. Yang, H.; Chen, Y.; Qin, Y. Application of atomic layer deposition in fabricating high-efficiency electrocatalysts. *Chin. J. Catal.* **2020**, *41*, 227–241. [[CrossRef](#)]
35. Yoo, C.; Jeon, J.W.; Yoon, S.; Cheng, Y.; Han, G.; Choi, W.; Park, B.; Jeon, G.; Jeon, S.; Kim, W.; et al. Atomic Layer Deposition of Sb₂Te₃/GeTe Superlattice Film and Its Melt-Quenching-Free Phase-Transition Mechanism for Phase-Change Memory. *Adv. Mater.* **2022**, *34*, 202207143. [[CrossRef](#)]
36. Plutnar, J.; Pumera, M. Applications of Atomic Layer Deposition in Design of Systems for Energy Conversion. *Small* **2021**, *17*, 202102088. [[CrossRef](#)]
37. Fonseca, J.; Lu, J. Single-Atom Catalysts Designed and Prepared by the Atomic Layer Deposition Technique. *ACS Catal.* **2021**, *11*, 7018–7059. [[CrossRef](#)]
38. Seenivasan, S.; Shim, K.I.; Lim, C.; Kavinkumar, T.; Sivagurunathan, A.T.; Han, J.W.; Kim, D.-H. Boosting Pseudocapacitive Behavior of Supercapattery Electrodes by Incorporating a Schottky Junction for Ultrahigh Energy Density. *Nano-Micro Lett.* **2023**, *15*, 62. [[CrossRef](#)]
39. Gupta, B.; Hossain, M.A.; Riaz, A.; Sharma, A.; Zhang, D.; Tan, H.H.; Jagadish, C.; Catchpole, K.; Hoex, B.; Karuturi, S. Recent Advances in Materials Design Using Atomic Layer Deposition for Energy Applications. *Adv. Funct. Mater.* **2021**, *32*, 202109105. [[CrossRef](#)]
40. Du, C.; Shi, S.; Chen, G.; Zhang, Y.; Wei, Q.; Li, L.; Wan, G.; Deng, Z.; Wu, Y.; Su, Y.; et al. Structurally stable Fe–Ni–Co phosphide/graphene and nitrogen-doped carbon/graphene constructed by atomic layer deposition for high-performance hybrid supercapacitor. *Mater. Today Energy* **2023**, *34*, 101287. [[CrossRef](#)]
41. Nishizawa, J.-I. Molecular Layer Epitaxy. *Appl. Surf. Sci.* **1994**, *79–80*, 1–11. [[CrossRef](#)]
42. George, S.M. Atomic Layer Deposition: An Overview. *Chem. Rev.* **2010**, *110*, 111–131. [[CrossRef](#)] [[PubMed](#)]
43. Macco, B.; Kessels, W.M.M. Atomic layer deposition of conductive and semiconductive oxides. *Appl. Phys. Rev.* **2022**, *9*, 116732. [[CrossRef](#)]
44. Kolhep, M.; Pantle, F.; Karlinger, M.; Wang, D.; Scherer, T.; Kübel, C.; Stutzmann, M.; Zacharias, M. Atomic Layer Deposition and Strain Analysis of Epitaxial GaN-ZnO Core–Shell Nanowires. *Nano Lett.* **2023**, *23*, 6920–6926. [[CrossRef](#)] [[PubMed](#)]
45. Zuo, Y.; Wang, Z.; Zhao, H.; Zhao, L.; Zhang, L.; Yi, B.; Bao, W.; Zhang, Y.; Su, L.; Yu, Y.; et al. Synthesis of a Spatially Confined, Highly Durable, and Fully Exposed Pd Cluster Catalyst via Sequential Site-Selective Atomic Layer Deposition. *ACS Appl. Mater. Interfaces* **2022**, *14*, 14466–14473. [[CrossRef](#)]
46. Jin, Y.; Yu, H.; Liang, X. Understanding the roles of atomic layer deposition in improving the electrochemical performance of lithium-ion batteries. *Appl. Phys. Rev.* **2021**, *8*, 031301. [[CrossRef](#)]
47. Jia, J.; Jiang, Z.; Ma, S.; Guo, S.; Wu, J.; Zhang, Y.; Cao, B.; Dong, J. Novel Strategy for High Efficient and Stable Perovskite Solar Cells through Atomic Layer Deposition. *ACS Appl. Mater. Interfaces* **2024**, *16*, 3576–3585. [[CrossRef](#)]
48. Wang, D.; Huang, Q.; Shi, W.; You, W.; Meyer, T.J. Application of Atomic Layer Deposition in Dye-Sensitized Photoelectrosynthesis Cells. *Trends Chem.* **2020**, *3*, 59–71. [[CrossRef](#)]

49. McNeary, W.W.; Tacey, S.A.; Lahti, G.D.; Conklin, D.R.; Unocic, K.A.; Tan, E.C.D.; Wegener, E.C.; Erden, T.E.; Moulton, S.; Gump, C.; et al. Atomic Layer Deposition with TiO₂ for Enhanced Reactivity and Stability of Aromatic Hydrogenation Catalysts. *ACS Catal.* **2021**, *11*, 8538–8549. [[CrossRef](#)]
50. Chen, R.; Cao, K.; Wen, Y.; Yang, F.; Wang, J.; Liu, X.; Shan, B. Atomic layer deposition in advanced display technologies: From photoluminescence to encapsulation. *Int. J. Extrem. Manuf.* **2024**, *6*, 022003. [[CrossRef](#)]
51. Guo, H.J.; Sun, Y.; Zhao, Y.; Liu, G.X.; Song, Y.X.; Wan, J.; Jiang, K.C.; Guo, Y.G.; Sun, X.; Wen, R. Surface Degradation of Single-crystalline Ni-rich Cathode and Regulation Mechanism by Atomic Layer Deposition in Solid-State Lithium Batteries. *Angew. Chem. Int. Ed.* **2022**, *61*, 202211626. [[CrossRef](#)] [[PubMed](#)]
52. Karimzadeh, S.; Safaei, B.; Yuan, C.; Jen, T.-C. Emerging Atomic Layer Deposition for the Development of High-Performance Lithium-Ion Batteries. *Electrochem. Energy Rev.* **2023**, *6*, 24. [[CrossRef](#)]
53. Cai, J.; Han, X.; Wang, X.; Meng, X. Atomic Layer Deposition of Two-Dimensional Layered Materials: Processes, Growth Mechanisms, and Characteristics. *Matter* **2020**, *2*, 587–630. [[CrossRef](#)]
54. Ghosh, S.; Pariari, D.; Behera, T.; Boix, P.P.; Ganesh, N.; Basak, S.; Vidhan, A.; Sarda, N.; Mora-Seró, I.; Chowdhury, A.; et al. Buried Interface Passivation of Perovskite Solar Cells by Atomic Layer Deposition of Al₂O₃. *ACS Energy Lett.* **2023**, *8*, 2058–2065. [[CrossRef](#)]
55. Ansari, M.Z.; Hussain, I.; Mohapatra, D.; Ansari, S.A.; Rahighi, R.; Nandi, D.K.; Song, W.; Kim, S.H. Atomic Layer Deposition—A Versatile Toolbox for Designing/Engineering Electrodes for Advanced Supercapacitors. *Adv. Sci.* **2023**, *11*, 202303055. [[CrossRef](#)]
56. Sivagurunathan, A.T.; Adhikari, S.; Kim, D.-H. Strategies and implications of atomic layer deposition in photoelectrochemical water splitting: Recent advances and prospects. *Nano Energy* **2021**, *83*, 105802. [[CrossRef](#)]
57. Gao, Z.; Zhang, C.; Gao, J.; Wang, Q.; Xu, G.; Cao, H.; Zhang, H. Nucleation and growth of low resistivity copper thin films on polyimide substrates by low-temperature atomic layer deposition. *Appl. Surf. Sci.* **2023**, *638*, 158072. [[CrossRef](#)]
58. Henning, A.; Bartl, J.D.; Zeidler, A.; Qian, S.; Bienek, O.; Jiang, C.M.; Paulus, C.; Rieger, B.; Stutzmann, M.; Sharp, I.D. Aluminum Oxide at the Monolayer Limit via Oxidant-Free Plasma-Assisted Atomic Layer Deposition on GaN. *Adv. Funct. Mater.* **2021**, *31*, 202101441. [[CrossRef](#)]
59. Asundi, A.S.; Raiford, J.A.; Bent, S.F. Opportunities for Atomic Layer Deposition in Emerging Energy Technologies. *ACS Energy Lett.* **2019**, *4*, 908–925. [[CrossRef](#)]
60. Xu, S.; Wang, Z.; Dull, S.; Liu, Y.; Lee, D.U.; Lezama Pacheco, J.S.; Orazov, M.; Vullum, P.E.; Dadlani, A.L.; Vinogradova, O.; et al. Direct Integration of Strained-Pt Catalysts into Proton-Exchange-Membrane Fuel Cells with Atomic Layer Deposition. *Adv. Mater.* **2021**, *33*, 202007885. [[CrossRef](#)]
61. Liu, X.; Yang, B.; Zhou, X.; Wu, M.; Spiecker, E.; Bachmann, J.; Hauke, F.; Hirsch, A.; Wei, T. Synergistic Combination of Reductive Covalent Functionalization and Atomic Layer Deposition—Towards Spatially Defined Graphene–Organic–Inorganic Heterostructures. *Angew. Chem. Int. Ed.* **2023**, *62*, 202314183. [[CrossRef](#)] [[PubMed](#)]
62. Yang, X.; Sun, P.; Zhang, H.; Xia, Z.; Waldman, R.Z.; Mane, A.U.; Elam, J.W.; Shao, L.; Darling, S.B. Polyphenol-Sensitized Atomic Layer Deposition for Membrane Interface Hydrophilization. *Adv. Funct. Mater.* **2020**, *30*, 201910062. [[CrossRef](#)]
63. Popov, G.; Bačić, G.; Mattinen, M.; Manner, T.; Lindström, H.; Seppänen, H.; Suikonen, S.; Vehkämäki, M.; Kemell, M.; Jalkanen, P.; et al. Atomic Layer Deposition of PbS Thin Films at Low Temperatures. *Chem. Mater.* **2020**, *32*, 8216–8228. [[CrossRef](#)]
64. Yang, X.; Sun, P.; Wen, Y.; Mane, A.U.; Elam, J.W.; Ma, J.; Liu, S.; Darling, S.B.; Shao, L. Protein-activated atomic layer deposition for robust crude-oil-repellent hierarchical nano-armored membranes. *Sci. Bull.* **2024**, *69*, 218–226. [[CrossRef](#)]
65. Zhang, H.; Marshall, C.L. Atomic layer deposition: Catalytic preparation and modification technique for the next generation. *Chin. J. Catal.* **2019**, *40*, 1311–1323. [[CrossRef](#)]
66. Guo, D.; Wan, Z.; Li, Y.; Xi, B.; Wang, C. TiN@Co_{5.47}N Composite Material Constructed by Atomic Layer Deposition as Reliable Electrocatalyst for Oxygen Evolution Reaction. *Adv. Funct. Mater.* **2020**, *31*, 202008511. [[CrossRef](#)]
67. Zhang, J.; Zhang, G.; Chen, Z.; Dai, H.; Hu, Q.; Liao, S.; Sun, S. Emerging applications of atomic layer deposition for lithium-sulfur and sodium-sulfur batteries. *Energy Storage Mater.* **2020**, *26*, 513–533. [[CrossRef](#)]
68. Coutancier, D.; Zhang, S.-T.; Bernardini, S.; Fournier, O.; Mathieu-Pennober, T.; Donsanti, F.; Tchernycheva, M.; Foldyna, M.; Schneider, N. ALD of ZnO:Ti: Growth Mechanism and Application as an Efficient Transparent Conductive Oxide in Silicon Nanowire Solar Cells. *ACS Appl. Mater. Interfaces* **2020**, *12*, 21036–21044. [[CrossRef](#)]
69. Yu, F.; Du, L.; Zhang, G.; Su, F.; Wang, W.; Sun, S. Electrode Engineering by Atomic Layer Deposition for Sodium-Ion Batteries: From Traditional to Advanced Batteries. *Adv. Funct. Mater.* **2019**, *30*, 201906890. [[CrossRef](#)]
70. Yang, X.; Martinson, A.B.F.; Elam, J.W.; Shao, L.; Darling, S.B. Water treatment based on atomically engineered materials: Atomic layer deposition and beyond. *Matter* **2021**, *4*, 3515–3548. [[CrossRef](#)]
71. McNeary, W.W.; Zaccarine, S.F.; Lai, A.; Linico, A.E.; Pylypenko, S.; Weimer, A.W. Improved durability and activity of Pt/C catalysts through atomic layer deposition of tungsten nitride and subsequent thermal treatment. *Appl. Catal. B: Environ.* **2019**, *254*, 587–593. [[CrossRef](#)]
72. Ngambou, M.W.N.; Pellet-Mary, C.; Brinza, O.; Antonino, A.; Hetet, G.; Tallaire, A.; Bénédic, F.; Achard, J. Improving NV centre density during diamond growth by CVD process using N₂O gas. *Diam. Relat. Mater.* **2022**, *123*, 108884. [[CrossRef](#)]
73. Mendhe, A.C.; Dhas, S.; Kim, Y.; Kim, D. Hierarchically structured Cu₂P₂O₇ nanoflakes as a binder-free electrodes for high-performance supercapacitors. *Chem. Eng. J.* **2024**, *496*, 153857. [[CrossRef](#)]

74. Zhou, H.; Zhu, G.; Dong, S.; Liu, P.; Lu, Y.; Zhou, Z.; Cao, S.; Zhang, Y.; Pang, H. Ethanol-Induced Ni^{2+} -Intercalated Cobalt Organic Frameworks on Vanadium Pentoxide for Synergistically Enhancing the Performance of 3D-Printed Micro-Supercapacitors. *Adv. Mater.* **2023**, *35*, 2211523. [CrossRef] [PubMed]
75. Anuar, N.; Yusop, S.N.; Roberts, K.J. Crystallisation of organic materials from the solution phase: A molecular, synthonic and crystallographic perspective. *Crystallogr. Rev.* **2022**, *28*, 97–215. [CrossRef]
76. Martínez-Puente, M.A.; Horley, P.; Aguirre-Tostado, F.S.; López-Medina, J.; Borbón-Nuñez, H.A.; Tiznado, H.; Susarrey-Arce, A.; Martínez-Guerra, E. ALD and PEALD deposition of HfO_2 and its effects on the nature of oxygen vacancies. *Mater. Sci. Eng. B* **2022**, *285*, 115964. [CrossRef]
77. Pan, H.; Wang, C.; Zhang, Z.; Li, Y.; Hou, X.; Zheng, W.; Liu, X.; Wan, Y.; Zhang, J. Oxygen vacancy-enriched ALD NiO sub-50 nm thin films for enhanced triethylamine detection. *Appl. Phys. Lett.* **2022**, *121*, 111603. [CrossRef]
78. Hsu, C.-H.; Chen, K.-T.; Lin, L.-Y.; Wu, W.-Y.; Liang, L.-S.; Gao, P.; Qiu, Y.; Zhang, X.-Y.; Huang, P.-H.; Lien, S.-Y.; et al. Tantalum-Doped TiO_2 Prepared by Atomic Layer Deposition and Its Application in Perovskite Solar Cells. *Nanomaterials* **2021**, *11*, 1504. [CrossRef]
79. Yang, F.; Yang, R.; Yan, L.; Liu, X.; Luo, X.; Zhang, L. In situ growth of porous TiO_2 with controllable oxygen vacancies on an atomic scale for highly efficient photocatalytic water splitting. *Catal. Sci. Technol.* **2020**, *10*, 5659–5665. [CrossRef]
80. Kao, E.; Yang, C.; Warren, R.; Kozinda, A.; Lin, L. ALD titanium nitride on vertically aligned carbon nanotube forests for electrochemical supercapacitors. *Sens. Actuators A: Phys.* **2016**, *240*, 160–166. [CrossRef]
81. Wang, K.; Paxson, A.; Valdez, T.I.; Erlat, A.; Lee, P.-C.; Yun, S.; Khajanji, P.; Zhang, Z.; Kummel, A.C.; Bandaru, P. Enhanced Corrosion Resistance in Aluminum-Based Electrolyzer Components via Stoichiometry Tuned Atomic Layer-Deposited TiO_x Films. *ACS Appl. Mater. Interfaces* **2024**, *16*, 35043–35052. [CrossRef] [PubMed]
82. Wang, J.; Ni, Y.; Li, X.; Jiang, X.; Jin, Q.; Zhang, X.; Wei, S.; Jin, H.; Yuan, T.; Zou, J.; et al. Enhancement of nitric oxide sensing performance via oxygen vacancy promotion on strontium-doped LaFeO_3 perovskites. *Sens. Actuators B: Chem.* **2024**, *417*, 136157. [CrossRef]
83. Li, Z.; Liu, X.; Zhou, M.; Zhang, S.; Cao, S.; Lei, G.; Lou, C.; Zhang, J. Plasma-induced oxygen vacancies enabled ultrathin ZnO films for highly sensitive detection of triethylamine. *J. Hazard. Mater.* **2021**, *415*, 125757. [CrossRef] [PubMed]
84. Hu, Q.; Wang, S.; Gao, Z.; Li, Y.; Zhang, Q.; Xiang, Q.; Qin, Y. The precise decoration of Pt nanoparticles with Fe oxide by atomic layer deposition for the selective hydrogenation of cinnamaldehyde. *Appl. Catal. B: Environ.* **2017**, *218*, 591–599. [CrossRef]
85. Cao, L.; Liu, W.; Luo, Q.; Yin, R.; Wang, B.; Weissenrieder, J.; Soldemo, M.; Yan, H.; Lin, Y.; Sun, Z.; et al. Atomically dispersed iron hydroxide anchored on Pt for preferential oxidation of CO in H_2 . *Nature* **2019**, *565*, 631–635. [CrossRef]
86. Hu, Q.; Lu, X.; Gao, T.; Zhang, J.; Dong, Z.; Ma, Z.; Wang, X.; Lu, B.; Lv, Z.; Xu, J. A novel Cu-doped ZnO confined structure: Precisely preparation, and sensitization mechanism for ppb-level H_2S gas detection. *Sens. Actuators B: Chem.* **2024**, *414*, 135852. [CrossRef]
87. Hu, Q.-M.; Dong, Z.; Zhang, G.-X.; Li, Y.-X.; Xing, S.-F.; Ma, Z.-H.; Dong, B.-Y.; Lu, B.; Sun, S.-H.; Xu, J.-Q. Ultra-thin ALD CoO_x - ZnO heterogenous films as highly sensitive and environmentally friendly H_2S sensor. *Rare Met.* **2023**, *42*, 3054–3063. [CrossRef]
88. Jiang, Y.; Wang, Z.; Xu, C.; Li, W.; Li, Y.; Huang, S.; Chen, Z.; Zhao, B.; Sun, X.; Wilkinson, D.P.; et al. Atomic layer deposition for improved lithophilicity and solid electrolyte interface stability during lithium plating. *Energy Storage Mater.* **2020**, *28*, 17–26. [CrossRef]
89. Guo, Y.; Wang, S.; Du, X.; Liang, S.; Huang, S.; Peng, S.; Xie, Y.; Ma, M.; Xiong, L. Construction of ultrahigh capacity density carbon nanotube based MIM capacitor. *Energy Storage Mater.* **2023**, *63*, 103064. [CrossRef]
90. Hossain, M.I.; Saleque, A.M.; Ahmed, S.; Saidjafarzoda, I.; Shahiduzzaman, M.; Qarony, W.; Knipp, D.; Biyikli, N.; Tsang, Y.H. Perovskite/perovskite planar tandem solar cells: A comprehensive guideline for reaching energy conversion efficiency beyond 30%. *Nano Energy* **2021**, *79*, 105400. [CrossRef]
91. Widiapradja, L.J.; Hong, S.; Kim, K.-T.; Bae, H.; Im, S. Van der Waals crystal radio with Pt/ MoSe_2 Schottky diode and h-BN capacitor for RF energy harvesting. *Nano Energy* **2022**, *92*, 106771. [CrossRef]
92. Wu, S.M.; Yang, X.Y.; Janiak, C. Confinement Effects in Zeolite-Confined Noble Metals. *Angew. Chem. Int. Ed.* **2019**, *58*, 12340–12354. [CrossRef]
93. Pan, X.; Bao, X. The Effects of Confinement inside Carbon Nanotubes on Catalysis. *Acc. Chem. Res.* **2011**, *44*, 553–562. [CrossRef] [PubMed]
94. Easun, T.L.; Moreau, F.; Yan, Y.; Yang, S.; Schröder, M. Structural and dynamic studies of substrate binding in porous metal–organic frameworks. *Chem. Soc. Rev.* **2017**, *46*, 239–274. [CrossRef] [PubMed]
95. Dong, Z.; Hu, Q.; Gao, T.; Wang, J.; Kong, J.; Li, J.; Mao, L.; Wu, C.; Xu, J. Confining isolated Pt atoms into the porous SnO_2 for efficient gas sensing. *Ceram. Int.* **2024**, *50*, 22220–22231. [CrossRef]
96. Hu, Q.; Wu, C.; Dong, Z.; Zhang, G.; Ma, Z.; Wang, X.; Sun, S.; Xu, J. Direct confirmation of confinement effects by NiO confined in helical SnO_2 nanocoils and its application in sensors. *J. Mater. Chem. A* **2022**, *10*, 2786–2794. [CrossRef]
97. Li, W.; Wang, D.; Zhang, Y.; Tao, L.; Wang, T.; Zou, Y.; Wang, Y.; Chen, R.; Wang, S. Defect Engineering for Fuel-Cell Electrocatalysts. *Adv. Mater.* **2020**, *32*, 201907879. [CrossRef]
98. Bai, S.; Zhang, N.; Gao, C.; Xiong, Y. Defect engineering in photocatalytic materials. *Nano Energy* **2018**, *53*, 296–336. [CrossRef]

99. Park, K.; Lee, J.-H.; Lee, J.-W. Surface Defect Engineering of Metal Halide Perovskites for Photovoltaic Applications. *ACS Energy Lett.* **2022**, *7*, 1230–1239. [[CrossRef](#)]
100. Ortiz-Medina, J.; Wang, Z.; Cruz-Silva, R.; Morelos-Gomez, A.; Wang, F.; Yao, X.; Terrones, M.; Endo, M. Defect Engineering and Surface Functionalization of Nanocarbons for Metal-Free Catalysis. *Adv. Mater.* **2019**, *31*, 201805717. [[CrossRef](#)]
101. Zeng, H.; Chen, H.; Yang, B.; Zeng, J.; Meng, L.; Shi, D.; Chen, L.; Huang, Y. Highly-oxidizing Au@MnO_{2-x} nanozymes mediated homogeneous electrochemical detection of organophosphorus independent of dissolved oxygen. *J. Hazard. Mater.* **2023**, *459*, 132116. [[CrossRef](#)] [[PubMed](#)]
102. Ma, Z.; Martins, S.; Tan, Z.; Chen, S.; Monteblanco, E.; Liedke, M.O.; Butterling, M.; Attallah, A.G.; Hirschmann, E.; Wagner, A.; et al. Controlling Magneto-Ionics by Defect Engineering Through Light Ion Implantation. *Adv. Funct. Mater.* **2024**, *34*, 202312827. [[CrossRef](#)]
103. Wu, G.; Wang, Q.; Wu, Y.; Sun, X.; Liao, J.; Pan, J.; Chen, M.; Kasu, M.; Liu, S. Evolution of defects, morphologies and fundamental growth characteristics of CVD diamond films induced by nitrogen addition. *Mater. Today Commun.* **2020**, *25*, 101504. [[CrossRef](#)]
104. Ling, W.; Wang, X.; Wang, L.; Wang, X.; Zhan, X. Defect formation mechanism of laser additive manufacturing joint for large-thickness Ti₆Al₄V titanium alloy with Y₂O₃ nanoparticles. *Opt. Laser Technol.* **2023**, *157*, 108648. [[CrossRef](#)]
105. Meng, L.; Tian, W.; Wu, F.; Cao, F.; Li, L. TiO₂ ALD decorated CuO/BiVO₄ p-n heterojunction for improved photoelectrochemical water splitting. *J. Mater. Sci. Technol.* **2019**, *35*, 1740–1746. [[CrossRef](#)]
106. Yu, X.; Liu, C.; Li, C.; Wang, C.; Li, Y.; Liang, L.; Yu, W.; Wang, Y.; Liu, C.; Liu, Y.; et al. Controlled NiO_x Defect Engineering to Harnessing Redox Reactions in Perovskite Photovoltaic Cells via Atomic Layer Deposition. *ACS Appl. Mater. Interfaces* **2024**, *16*, 31114–31125. [[CrossRef](#)]
107. Dai, B.; Wu, C.; Xie, Y. Boosting the electrochromic performance of TiO₂ nanowire film via successively evolving surface structure. *Sci. China Chem.* **2021**, *64*, 745–752. [[CrossRef](#)]
108. Xiong, S.; Hou, Z.; Zou, S.; Lu, X.; Yang, J.; Hao, T.; Zhou, Z.; Xu, J.; Zeng, Y.; Xiao, W.; et al. Direct Observation on p- to n-Type Transformation of Perovskite Surface Region during Defect Passivation Driving High Photovoltaic Efficiency. *Joule* **2021**, *5*, 467–480. [[CrossRef](#)]
109. Zhou, L.; Zhang, L.; Li, H.; Shen, W.; Li, M.; He, R. Defect Passivation in Air-Stable Tin(IV)-Halide Single Crystal for Emissive Self-Trapped Excitons. *Adv. Funct. Mater.* **2021**, *31*, 202108561. [[CrossRef](#)]
110. Feng, W.; Zhao, Y.; Lin, K.; Lu, J.; Liang, Y.; Liu, K.; Xie, L.; Tian, C.; Lyu, T.; Wei, Z. Polymer-Assisted Crystal Growth Regulation and Defect Passivation for Efficient Perovskite Light-Emitting Diodes. *Adv. Funct. Mater.* **2022**, *32*, 202203371. [[CrossRef](#)]
111. Xu, T.; Xie, Y.; Qi, S.; Zhang, H.; Ma, W.; Wang, J.; Gao, Y.; Wang, L.; Zong, X. Simultaneous Defect Passivation and Co-Catalyst Engineering Leads to Superior Photocatalytic Hydrogen Evolution on Metal Halide Perovskites. *Angew. Chem. Int. Ed.* **2024**, *63*, 202409945. [[CrossRef](#)] [[PubMed](#)]
112. Jung, S.M.; Kang, H.L.; Won, J.K.; Kim, J.; Hwang, C.; Ahn, K.; Chung, I.; Ju, B.-K.; Kim, M.-G.; Park, S.K. High-Performance Quantum Dot Thin-Film Transistors with Environmentally Benign Surface Functionalization and Robust Defect Passivation. *ACS Appl. Mater. Interfaces* **2018**, *10*, 3739–3749. [[CrossRef](#)] [[PubMed](#)]
113. Jesna, G.K.; Halali, V.V.; Sanjayan, C.G.; Suvina, V.; Sakar, M.; Balakrishna, R.G. Perovskite nanomaterials as optical and electrochemical sensors. *Inorg. Chem. Front.* **2020**, *7*, 2702–2725. [[CrossRef](#)]
114. Li, Y.; Wu, F.; Han, M.; Li, Z.; Zhu, L.; Li, Z. Merocyanine with Hole-Transporting Ability and Efficient Defect Passivation Effect for Perovskite Solar Cells. *ACS Energy Lett.* **2021**, *6*, 869–876. [[CrossRef](#)]
115. Nam, T.; Lee, H.; Seo, S.; Cho, S.M.; Shong, B.; Lee, H.-B.-R.; Kim, H. Moisture barrier properties of low-temperature atomic layer deposited Al₂O₃ using various oxidants. *Ceram. Int.* **2019**, *45*, 19105–19112. [[CrossRef](#)]
116. Kim, S.; Lee, S.-H.; Jo, I.H.; Park, T.J.; Kim, J.H. Reduced leakage current in atomic-layer-deposited HfO₂ thin films deposited at low temperature by in-situ defect passivation. *Appl. Surf. Sci.* **2024**, *645*, 158790. [[CrossRef](#)]
117. Ng, S.; Iffelsberger, C.; Michalička, J.; Pumera, M. Atomic Layer Deposition of Electrocatalytic Insulator Al₂O₃ on Three-Dimensional Printed Nanocarbons. *ACS Nano* **2021**, *15*, 686–697. [[CrossRef](#)]
118. Jayaraman, S.; Rawson, T.J.; Belyustina, M.A. Designing supercapacitor electrolyte via ion counting. *Energy Environ. Sci.* **2022**, *15*, 2948–2957. [[CrossRef](#)]
119. Tang, Y.; Guo, W.; Zou, R. Nickel-based bimetallic battery-type materials for asymmetric supercapacitors. *Coord. Chem. Rev.* **2022**, *451*, 214242. [[CrossRef](#)]
120. Zhou, Y.; Qi, H.; Yang, J.; Bo, Z.; Huang, F.; Islam, M.S.; Lu, X.; Dai, L.; Amal, R.; Wang, C.H.; et al. Two-birds-one-stone: Multifunctional supercapacitors beyond traditional energy storage. *Energy Environ. Sci.* **2021**, *14*, 1854–1896. [[CrossRef](#)]
121. Patil, S.J.; Chodankar, N.R.; Hwang, S.-K.; Raju, G.S.R.; Ranjith, K.S.; Huh, Y.S.; Han, Y.-K. Ultra-stable flexible Zn-ion capacitor with pseudocapacitive 2D layered niobium oxyphosphides. *Energy Storage Mater.* **2022**, *45*, 1040–1051. [[CrossRef](#)]
122. Zhang, Y.; Mei, H.-X.; Cao, Y.; Yan, X.-H.; Yan, J.; Gao, H.-L.; Luo, H.-W.; Wang, S.-W.; Jia, X.-D.; Kachalova, L.; et al. Recent advances and challenges of electrode materials for flexible supercapacitors. *Coord. Chem. Rev.* **2021**, *438*, 213910. [[CrossRef](#)]
123. Xu, M.; Huang, Y.; Chen, R.; Huang, Q.; Yang, Y.; Zhong, L.; Ren, J.; Wang, X. Green conversion of Ganoderma lucidum residues to electrode materials for supercapacitors. *Adv. Compos. Hybrid Mater.* **2021**, *4*, 1270–1280. [[CrossRef](#)]
124. Ma, Y.; Xie, X.; Yang, W.; Yu, Z.; Sun, X.; Zhang, Y.; Yang, X.; Kimura, H.; Hou, C.; Guo, Z.; et al. Recent advances in transition metal oxides with different dimensions as electrodes for high-performance supercapacitors. *Adv. Compos. Hybrid Mater.* **2021**, *4*, 906–924. [[CrossRef](#)]

125. Sowbakkiyavathi, E.S.; Arunachala Kumar, S.P.; Maurya, D.K.; Balakrishnan, B.; Guo, J.Z.; Subramania, A. Research progress in the development of transition metal chalcogenides and their composite-based electrode materials for supercapacitors. *Adv. Compos. Hybrid Mater.* **2024**, *7*, 130. [[CrossRef](#)]
126. Kavinkumar, T.; Seenivasan, S.; Sivagurunathan, A.T.; Kwon, Y.; Kim, D.-H. Three-Dimensional Hierarchical Core/shell Electrodes Using Highly Conformal TiO_2 and Co_3O_4 Thin Films for High-Performance Supercapattery Devices. *ACS Appl. Mater. Interfaces* **2021**, *13*, 29058–29069. [[CrossRef](#)]
127. Naeem, F.; Naeem, S.; Zhao, Z.; Shu, G.-Q.; Zhang, J.; Mei, Y.; Huang, G. Atomic layer deposition synthesized ZnO nanomembranes: A facile route towards stable supercapacitor electrode for high capacitance. *J. Power Sources* **2020**, *451*, 227740. [[CrossRef](#)]
128. Li, Z.; Su, J.; Wang, X. Atomic layer deposition in the development of supercapacitor and lithium-ion battery devices. *Carbon* **2021**, *179*, 299–326. [[CrossRef](#)]
129. Chodankar, N.R.; Selvaraj, S.; Ji, S.H.; Kwon, Y.; Kim, D.H. Interface-Engineered Nickel Cobaltite Nanowires through NiO Atomic Layer Deposition and Nitrogen Plasma for High-Energy, Long-Cycle-Life Foldable All-Solid-State Supercapacitors. *Small* **2018**, *15*, 1803716. [[CrossRef](#)]
130. Jayaraman, V.; Sivagurunathan, A.T.; Adhikari, S.; Kim, D.H. $\text{CoO}_x@\text{NiMoN}/\text{Ti}_3\text{C}_2\text{T}_x$ Interface for Stable High-Performance Electrochemical Energy Storage Devices. *Small* **2023**, *20*, 2305868. [[CrossRef](#)]
131. Saha, A.; Shalev, O.; Maiti, S.; Wang, L.; Akella, S.H.; Schmerling, B.; Targin, S.; Tkachev, M.; Fan, X.; Noked, M. Evolution of ternary $\text{Li}_x\text{Sn}_y\text{O}_z$ artificial cathode-electrolyte interphase (ACEI) through ALD: A surface strengthened NCM811 with enhanced electrochemical performances for Li-ion batteries. *Mater. Today Energy* **2023**, *31*, 101207. [[CrossRef](#)]
132. Zyulkov, I.; Madhiwala, V.; Voronina, E.; Snelgrove, M.; Bogan, J.; O'Connor, R.; De Gendt, S.; Armini, S. Area-Selective ALD of Ru on Nanometer-Scale Cu Lines through Dimerization of Amino-Functionalized Alkoxy Silane Passivation Films. *ACS Appl. Mater. Interfaces* **2020**, *12*, 4678–4688. [[CrossRef](#)] [[PubMed](#)]
133. Multia, J.; Heiska, J.; Khayyami, A.; Karppinen, M. Electrochemically Active In Situ Crystalline Lithium-Organic Thin Films by ALD/MLD. *ACS Appl. Mater. Interfaces* **2020**, *12*, 41557–41566. [[CrossRef](#)] [[PubMed](#)]
134. Azaceta, E.; García, S.; Leonet, O.; Beltrán, M.; Gómez, I.; Chuvilin, A.; Mainar, A.R.; Blazquez, J.A.; Knez, M. Particle atomic layer deposition as an effective way to enhance Li-S battery energy density. *Mater. Today Energy* **2020**, *18*, 100567. [[CrossRef](#)]
135. Spurling, D.; Krüger, H.; Kohlmann, N.; Rasch, F.; Kremer, M.P.; Kienle, L.; Adelung, R.; Nicolosi, V.; Schütt, F. 3D networked MXene thin films for high performance supercapacitors. *Energy Storage Mater.* **2024**, *65*, 103148. [[CrossRef](#)]
136. Lin, D.; Qian, O.; Huo, D.; Pan, Q.; Zhang, S.; Wang, Z.; Han, F.; Wei, B. Alternately stacked thin film electrodes for high-performance compact energy storage. *Nano Energy* **2020**, *78*, 105323. [[CrossRef](#)]
137. Li, H.; Liu, Y.; Lin, S.; Li, H.; Wu, Z.; Zhu, L.; Li, C.; Wang, X.; Zhu, X.; Sun, Y. Laser crystallized sandwich-like MXene/ Fe_3O_4 /MXene thin film electrodes for flexible supercapacitors. *J. Power Sources* **2021**, *497*, 229882. [[CrossRef](#)]
138. Bhosale, R.P.; Kumbhar, S.S.; Bhosale, S.B.; Salunkhe, R.R.; Kadam, V.A.; Pardhi, S.P.; Gholap, S.S.; Lokhande, C.D.; Jamadade, V.S. Morphology modulation of MnFe_2O_4 thin film electrode for enhanced performance of hybrid supercapacitor. *J. Energy Storage* **2024**, *86*, 111146. [[CrossRef](#)]
139. Liang, Q.; Wang, Y.; Yang, Y.; Xu, T.; Xu, Y.; Zhao, Q.; Heo, S.-H.; Kim, M.-S.; Jeong, Y.-H.; Yao, S.; et al. Nanocellulose/two dimensional nanomaterials composites for advanced supercapacitor electrodes. *Front. Bioeng. Biotechnol.* **2022**, *10*, 1024453. [[CrossRef](#)]
140. Kim, M.-J.; Bae, J.-S.; Jung, M.-J.; Jeon, E.; Park, Y.; Khan, H.; Kwon, S.-H. Atomic Layer Deposition of Defective Amorphous TiO_x Thin Films with Improved Photoelectrochemical Performance. *ACS Appl. Mater. Interfaces* **2023**, *15*, 45732–45744. [[CrossRef](#)]
141. Giraldo, B.; Fryauf, D.M.; Cheney, B.; Sands, J.H.; Kobayashi, N.P. Demonstration of Sputtering Atomic Layer Augmented Deposition: Aluminum Oxide–Copper Dielectric–Metal Nanocomposite Thin Films. *ACS Appl. Mater. Interfaces* **2020**, *12*, 14280–14288. [[CrossRef](#)] [[PubMed](#)]
142. Park, H.; Hwang, J.H.; Oh, S.H.; Ryu, J.J.; Jeon, K.; Kang, M.; Chai, H.-J.; Ham, A.; Kim, G.H.; Kang, K.; et al. Direct Growth of Bi_2SeO_5 Thin Films for High-k Dielectrics via Atomic Layer Deposition. *ACS Nano* **2024**, *18*, 22071–22079. [[CrossRef](#)] [[PubMed](#)]
143. Lopa, N.S.; Akbari, M.K.; Lu, H.L.; Zhuiykov, S. ALD-enabled $\text{WO}_3\text{-MoO}_3$ nanohybrid heterostructure for high-performance electrochemical supercapacitors. *J. Energy Storage* **2024**, *84*, 110777. [[CrossRef](#)]
144. Lopa, N.S.; Akbari, M.K.; Wu, D.; Verpoort, F.; Zhuiykov, S. Two-Dimensional $\text{SnO}_2\text{-ZnO}$ Nanohybrid Electrode Fabricated via Atomic Layer Deposition for Electrochemical Supercapacitors. *Energy Fuels* **2023**, *37*, 3142–3151. [[CrossRef](#)]
145. Lopa, N.S.; Akbari, M.K.; Zhuiykov, S. ALD-fabricated two-dimensional $\text{SnO}_2\text{-In}_2\text{O}_3$ n-n nanohybrid electrode for electrochemical supercapacitors. *Electrochim. Acta* **2022**, *434*, 141322. [[CrossRef](#)]
146. Ye, F.; Xu, B.; Chen, R.; Li, R.; Chang, G. A high performance flexible cotton-based supercapacitor prepared by in-situ polyaniline and MXene coating. *J. Energy Storage* **2023**, *62*, 106803. [[CrossRef](#)]
147. Dharmasiri, B.; Usman, K.A.S.; Qin, S.A.; Razal, J.M.; Tran, N.T.; Coia, P.; Harte, T.; Henderson, L.C. $\text{Ti}_3\text{C}_2\text{T}_x$ MXene coated carbon fibre electrodes for high performance structural supercapacitors. *Chem. Eng. J.* **2023**, *476*, 146739. [[CrossRef](#)]
148. Baig, M.M.; Khan, M.A.; Gul, I.H.; Rehman, S.U.; Shahid, M.; Javaid, S.; Baig, S.M. A Review of Advanced Electrode Materials for Supercapacitors: Challenges and Opportunities. *J. Electron. Mater.* **2023**, *52*, 5775–5794. [[CrossRef](#)]
149. Etman, A.S.; Halim, J.; Rosen, J. MXene-based Zn-ion hybrid supercapacitors: Effects of anion carriers and MXene surface coatings on the capacities and life span. *J. Energy Storage* **2022**, *52*, 104823. [[CrossRef](#)]

150. Dong, W.; Lin, T.; Huang, J.; Wang, Y.; Zhang, Z.; Wang, X.; Yuan, X.; Lin, J.; Chen, I.W.; Huang, F. Electrodes with Electrodeposited Water-excluding Polymer Coating Enable High-Voltage Aqueous Supercapacitors. *Research* **2020**, *2020*, 4178179. [\[CrossRef\]](#)
151. Kim, H.; Maity, C.K.; Venkateswarlu, S.; Kim, M.J. Alternative inner filling and outer surface coating of BNNT by Tungsten(VI) oxide for supercapacitor electrode. *Compos. Part B: Eng.* **2024**, *279*, 111436. [\[CrossRef\]](#)
152. Liu, X.; Li, J.; Liu, Y.; Zhou, L. Achieving enhanced multifunctional performance for structural composite supercapacitors by reinforcing interfaces with polymer coating. *J. Colloid Interface Sci.* **2024**, *665*, 603–612. [\[CrossRef\]](#) [\[PubMed\]](#)
153. Hsain, H.A.; Lee, Y.; Lancaster, S.; Materano, M.; Alcala, R.; Xu, B.; Mikolajick, T.; Schroeder, U.; Parsons, G.N.; Jones, J.L. Role of Oxygen Source on Buried Interfaces in Atomic-Layer-Deposited Ferroelectric Hafnia–Zirconia Thin Films. *ACS Appl. Mater. Interfaces* **2022**, *14*, 42232–42244. [\[CrossRef\]](#) [\[PubMed\]](#)
154. Ahaliabadeh, Z.; Miikkulainen, V.; Mäntymäki, M.; Colalongo, M.; Mousavihasemi, S.; Yao, L.; Jiang, H.; Lahtinen, J.; Kankaanpää, T.; Kallio, T. Stabilized Nickel-Rich-Layered Oxide Electrodes for High-Performance Lithium-Ion Batteries. *Energy Environ. Mater.* **2024**, *7*, 12741. [\[CrossRef\]](#)
155. Adhikari, S.; Selvaraj, S.; Ji, S.H.; Kim, D.H. Encapsulation of Co_3O_4 Nanocone Arrays via Ultrathin NiO for Superior Performance Asymmetric Supercapacitors. *Small* **2020**, *16*, 202005414. [\[CrossRef\]](#)
156. Wang, H.; Niu, H.; Wang, H.; Wang, W.; Jin, X.; Wang, H.; Zhou, H.; Lin, T. Micro-meso porous structured carbon nanofibers with ultra-high surface area and large supercapacitor electrode capacitance. *J. Power Sources* **2021**, *482*, 228986. [\[CrossRef\]](#)
157. Bian, Z.; Wang, Y.; Zhu, B.; Ye, R.; Yuan, F.; Zhang, Y.; Liu, T.; Zhang, P.; Chen, C.; Zhu, G.; et al. Converting Hippophae rhamnoides fruit extraction residue into porous carbons with ultra-high surface area for superior-performance supercapacitors. *J. Energy Storage* **2024**, *98*, 113058. [\[CrossRef\]](#)
158. Pawar, S.A.; Patil, D.S.; Nandi, D.K.; Monirul Islam, M.; Sakurai, T.; Kim, S.-H.; Shin, J.C. Cobalt-based metal oxide coated with ultrathin ALD- MoS_2 as an electrode material for supercapacitors. *Chem. Eng. J.* **2022**, *435*, 135066. [\[CrossRef\]](#)
159. Sahoo, B.B.; Kumar, N.; Panda, H.S.; Panigrahy, B.; Sahoo, N.K.; Soam, A.; Mahanto, B.S.; Sahoo, P.K. Self-assembled 3D graphene-based aerogel with Au nanoparticles as high-performance supercapacitor electrode. *J. Energy Storage* **2021**, *43*, 103157. [\[CrossRef\]](#)
160. Zhao, Y.; Wang, S.; Yuan, M.; Chen, Y.; Huang, Y.; Lian, J.; Yang, S.; Li, H.; Wu, L. Amorphous MoS nanoparticles grown on cobalt-iron-based needle-like array for high-performance flexible asymmetric supercapacitor. *Chem. Eng. J.* **2021**, *417*, 127927. [\[CrossRef\]](#)
161. Karim, M.R.; Mohammad, A.; Mukta, C.B.; Lee, J.; Yoon, T. Biofilm-engineered fabrication of Ag nanoparticles with modified ZIF-8-derived ZnO for a high-performance supercapacitor. *J. Energy Storage* **2024**, *75*, 109646. [\[CrossRef\]](#)
162. Albashir, A.I.M.; Shang, W.; Hadi, M.K.; Zhang, J.; Zhang, T.; Ran, F. Straightforward Solution Polymerization Synthesis of Porous Carbon@Gold Nanoparticles Electrode for High-Performance Supercapacitor. *J. Energy Storage* **2021**, *33*, 102041. [\[CrossRef\]](#)
163. Zhang, Y.; Cao, J.; Yuan, Z.; Zhao, L.; Wang, L.; Han, W. Assembling Co_3O_4 Nanoparticles into MXene with Enhanced electrochemical performance for advanced asymmetric supercapacitors. *J. Colloid Interface Sci.* **2021**, *599*, 109–118. [\[CrossRef\]](#) [\[PubMed\]](#)
164. Ma, Q.; Liu, M.; Cui, F.; Zhang, J.; Cui, T. Fabrication of 3D graphene microstructures with uniform metal oxide nanoparticles via molecular self-assembly strategy and their supercapacitor performance. *Carbon* **2023**, *204*, 336–345. [\[CrossRef\]](#)
165. Jiang, H.; Yan, X.; Miao, J.; You, M.; Zhu, Y.; Pan, J.; Wang, L.; Cheng, X. Super-conductive silver nanoparticles functioned three-dimensional Cu_xO foams as a high-pseudocapacitive electrode for flexible asymmetric supercapacitors. *J. Mater.* **2021**, *7*, 156–165. [\[CrossRef\]](#)
166. Hai, Z.; Karbalaei Akbari, M.; Wei, Z.; Xue, C.; Xu, H.; Hu, J.; Hyde, L.; Zhuiykov, S. TiO_2 nanoparticles-functionalized two-dimensional WO_3 for high-performance supercapacitors developed by facile two-step ALD process. *Mater. Today Commun.* **2017**, *12*, 55–62. [\[CrossRef\]](#)
167. Nandi, D.K.; Sahoo, S.; Sinha, S.; Yeo, S.; Kim, H.; Bulakhe, R.N.; Heo, J.; Shim, J.-J.; Kim, S.-H. Highly Uniform Atomic Layer-Deposited MoS_2 @3D-Ni-Foam: A Novel Approach To Prepare an Electrode for Supercapacitors. *ACS Appl. Mater. Interfaces* **2017**, *9*, 40252–40264. [\[CrossRef\]](#)
168. Ramadoss, A.; Kim, T.; Kim, G.-S.; Kim, S.J. Enhanced activity of a hydrothermally synthesized mesoporous MoS_2 nanostructure for high performance supercapacitor applications. *New J. Chem.* **2014**, *38*, 2379–2385. [\[CrossRef\]](#)
169. Nardekar, S.S.; Krishnamoorthy, K.; Pazhamalai, P.; Sahoo, S.; Mariappan, V.K.; Kim, S.-J. Exceptional interfacial electrochemistry of few-layered 2D MoS_2 quantum sheets for high performance flexible solid-state supercapacitors. *J. Mater. Chem. A* **2020**, *8*, 13121–13131. [\[CrossRef\]](#)
170. Li, H.; Gao, Y.; Shao, Y.; Su, Y.; Wang, X. Vapor-Phase Atomic Layer Deposition of Co_9S_8 and Its Application for Supercapacitors. *Nano Lett.* **2015**, *15*, 6689–6695. [\[CrossRef\]](#)
171. Zhang, N.; Wang, W.; Teng, C.; Wu, Z.; Ye, Z.; Zhi, M.; Hong, Z. Co_9S_8 nanoparticle-decorated carbon nanofibers as high-performance supercapacitor electrodes. *RSC Adv.* **2018**, *8*, 27574–27579. [\[CrossRef\]](#) [\[PubMed\]](#)
172. Lin, T.W.; Tsai, H.C.; Chen, T.Y.; Shao, L.D. Facile and Controllable One-Pot Synthesis of Hierarchical Co_9S_8 Hollow Microspheres as High-Performance Electroactive Materials for Energy Storage and Conversion. *ChemElectroChem* **2017**, *5*, 137–143. [\[CrossRef\]](#)
173. Naeem, F.; Naeem, S.; Zhao, Y.; Wang, D.; Zhang, J.; Mei, Y.; Huang, G. TiO_2 Nanomembranes Fabricated by Atomic Layer Deposition for Supercapacitor Electrode with Enhanced Capacitance. *Nanoscale Res. Lett.* **2019**, *14*, 92. [\[CrossRef\]](#)

174. Zhang, Y.; Wang, F.; Zhu, H.; Zhang, D.; Chen, J. Elongated TiO₂ nanotubes directly grown on graphene nanosheets as an efficient material for supercapacitors and absorbents. *Compos. Part A: Appl. Sci. Manuf.* **2017**, *101*, 297–305. [CrossRef]
175. Ambade, R.B.; Ambade, S.B.; Shrestha, N.K.; Salunkhe, R.R.; Lee, W.; Bagde, S.S.; Kim, J.H.; Stadler, F.J.; Yamauchi, Y.; Lee, S.-H. Controlled growth of polythiophene nanofibers in TiO₂ nanotube arrays for supercapacitor applications. *J. Mater. Chem. A* **2017**, *5*, 172–180. [CrossRef]
176. Daubert, J.S.; Lewis, N.P.; Gotsch, H.N.; Mundy, J.Z.; Monroe, D.N.; Dickey, E.C.; Losego, M.D.; Parsons, G.N. Effect of Meso- and Micro-Porosity in Carbon Electrodes on Atomic Layer Deposition of Pseudocapacitive V₂O₅ for High Performance Supercapacitors. *Chem. Mater.* **2015**, *27*, 6524–6534. [CrossRef]
177. Prakash, H.C.; Kumar, M.S.; Lin, T.-W.; Batabyal, S.K. Photo-assisted capacitive performance of V₂O₅ supercapacitor. *Electrochim. Acta* **2023**, *469*, 143229. [CrossRef]
178. Karade, S.S.; Lalwani, S.; Eum, J.-H.; Kim, H. Coin cell fabricated symmetric supercapacitor device of two-steps synthesized V₂O₅ Nanorods. *J. Electroanal. Chem.* **2020**, *864*, 114080. [CrossRef]
179. Warren, R.; Sammoura, F.; Tounsi, F.; Sanghadasa, M.; Lin, L. Highly active ruthenium oxide coating via ALD and electrochemical activation in supercapacitor applications. *J. Mater. Chem. A* **2015**, *3*, 15568–15575. [CrossRef]
180. Zhang, Q.; Hu, Z.; Yang, Y.; Zhang, Z.; Wang, X.; Yang, X.; An, Y.; Guo, B. Metal organic frameworks-derived porous carbons/ruthenium oxide composite and its application in supercapacitor. *J. Alloys Compd.* **2018**, *735*, 1673–1681. [CrossRef]
181. B, N.; Y, V.; Abdul Razack, S. Enhanced formation of ruthenium oxide nanoparticles through green synthesis for highly efficient supercapacitor applications. *Adv. Powder Technol.* **2020**, *31*, 1001–1006. [CrossRef]
182. Yu, L.; Wan, G.; Qin, Y.; Wang, G. Atomic layer deposition assisted fabrication of high-purity carbon nanocoil for electrochemical energy storage. *Electrochim. Acta* **2018**, *268*, 283–294. [CrossRef]
183. Liu, T.; Jiang, C.; Cheng, B.; You, W.; Yu, J. Hierarchical flower-like C/NiO composite hollow microspheres and its excellent supercapacitor performance. *J. Power Sources* **2017**, *359*, 371–378. [CrossRef]
184. Li, X.; Li, J.; Zhang, Y.; Zhao, P. Synthesis of Ni-MOF derived NiO/rGO composites as novel electrode materials for high performance supercapacitors. *Colloids Surf. A: Physicochem. Eng. Asp.* **2021**, *622*, 126653. [CrossRef]
185. Qiu, J.; Bai, Z.; Dai, E.; Liu, S.; Liu, Y. NiO/Co₃O₄ nanoheterostructure derived from nickelocene filled ZIF-67 for supercapacitors. *J. Alloys Compd.* **2018**, *763*, 966–974. [CrossRef]
186. Li, H.; Mi, W.; Zhang, F.; Song, Y.; Zhao, J. Microwave-assisted hydrothermal synthesis of NiO/Co₃O₄ nanosheets decorated on three-dimensional porous graphene for supercapacitors. *J. Phys. Chem. Solids* **2024**, *190*, 112025. [CrossRef]
187. Xiong, W.; Guo, Q.; Guo, Z.; Li, H.; Zhao, R.; Chen, Q.; Liu, Z.; Wang, X. Atomic layer deposition of nickel carbide for supercapacitors and electrocatalytic hydrogen evolution. *J. Mater. Chem. A* **2018**, *6*, 4297–4304. [CrossRef]
188. Liu, M.; Niu, B.; Guo, H.; Ying, S.; Chen, Z. Simple preparation of g-C₃N₄@Ni₃C nanosheets and its application in supercapacitor electrode materials, hydrogengeneration via NaBH₄ hydrolysis and reduction of p-nitrophenol. *Inorg. Chem. Commun.* **2021**, *130*, 108687. [CrossRef]
189. Liu, M.-C.; Hu, Y.-M.; An, W.-Y.; Kong, L.-B.; Kang, L. Liquid phase synthesis of dendritic nickel carbide alloy with high conductivity for advanced energy storage. *J. Energy Chem.* **2017**, *26*, 750–756. [CrossRef]
190. Ramachandran, T.; Hamed, F.; Raji, R.K.; Majhi, S.M.; Barik, D.; Kumar, Y.A.; Jauhar, R.M.; Pachamuthu, M.P.; Vijayalakshmi, L.; Ansar, S. Enhancing asymmetric supercapacitor performance with NiCo₂O₄–NiO hybrid electrode fabrication. *J. Phys. Chem. Solids* **2023**, *180*, 111467. [CrossRef]
191. Yao, D.; Ouyang, Y.; Jiao, X.; Ye, H.; Lei, W.; Xia, X.; Lu, L.; Hao, Q. Hierarchical NiO@NiCo₂O₄ Core–shell Nanosheet Arrays on Ni Foam for High-Performance Electrochemical Supercapacitors. *Ind. Eng. Chem. Res.* **2018**, *57*, 6246–6256. [CrossRef]
192. Xiang, K.; Wu, D.; Fan, Y.; You, W.; Zhang, D.; Luo, J.-L.; Fu, X.-Z. Enhancing bifunctional electrodes of oxygen vacancy abundant ZnCo₂O₄ nanosheets for supercapacitor and oxygen evolution. *Chem. Eng. J.* **2021**, *425*, 130583. [CrossRef]
193. Li, T.; Hu, Y.; Zhang, J.; Li, H.; Fang, K.; Wang, J.; Wang, Z.; Xu, M.; Zhao, B. Doping effect and oxygen vacancy engineering in nickel-manganese layered double hydroxides for high-performance supercapacitors. *Nano Energy* **2024**, *126*, 109690. [CrossRef]
194. Yue, J.; Lu, G.; Zhang, P.; Wu, Y.; Cheng, Z.; Kang, X. Oxygen vacancies modulation in graphene/MnO_x composite for high performance supercapacitors. *Colloids Surf. A: Physicochem. Eng. Asp.* **2019**, *569*, 10–17. [CrossRef]
195. Xu, L.; Xi, Y.; Huang, C.; Zhang, J.; Hua, Z.; Zhou, J.-J.; Yin, J.; Zhang, L.; Li, W.; Wang, J.; et al. Superior electronic/ionic transport dynamics of Zn-Co-OH/MnO₂ heterointerface containing oxygen vacancies for pseudocapacitive storage. *Chem. Eng. J.* **2023**, *468*, 143551. [CrossRef]
196. Feng, Y.; Liu, W.; Wang, Y.; Gao, W.; Li, J.; Liu, K.; Wang, X.; Jiang, J. Oxygen vacancies enhance supercapacitive performance of CuCo₂O₄ in high-energy-density asymmetric supercapacitors. *J. Power Sources* **2020**, *458*, 228005. [CrossRef]
197. Zhu, Z.; Tian, W.; Lv, X.; Wang, F.; Hu, Z.; Ma, K.; Wang, C.; Yang, T.; Ji, J. P-doped cobalt carbonate hydroxide@NiMoO₄ double-shelled hierarchical nanoarrays anchored on nickel foam as a bi-functional electrode for energy storage and conversion. *J. Colloid Interface Sci.* **2021**, *587*, 855–863. [CrossRef] [PubMed]
198. Zhang, H.; Bai, Y.; Chen, H.; Wu, J.; Li, C.M.; Su, X.; Zhang, L. Oxygen-defect-rich 3D porous cobalt-gallium layered double hydroxide for high-performance supercapacitor application. *J. Colloid Interface Sci.* **2022**, *608*, 1837–1845. [CrossRef]
199. Ramadan, A.; Ramadan, W. Superior performance of asymmetric supercapacitor based on Cu doped bismuth ferrite electrode. *J. Energy Storage* **2024**, *100*, 113702. [CrossRef]

200. Chen, Y.; Zhou, C.; Liu, G.; Kang, C.; Ma, L.; Liu, Q. Hydroxide ion dependent α -MnO₂ enhanced via oxygen vacancies as the negative electrode for high-performance supercapacitors. *J. Mater. Chem. A* **2021**, *9*, 2872–2887. [CrossRef]
201. Su, J.; Yang, L.; Yu, D.; Dong, S. Exploring the potential of constructing a hybrid supercapacitor with FeCoNi-LDH porous material containing oxygen vacancies for high-performance energy storage applications. *Nano Res.* **2024**, *17*, 8134–8144. [CrossRef]
202. Wang, C.; Wu, X.; Qin, Y.; Kong, Y. Reduced Mo-doped NiCo₂O₄ with rich oxygen vacancies as an advanced electrode material in supercapacitors. *Chem. Commun.* **2022**, *58*, 5120–5123. [CrossRef]
203. Wang, S.; Ding, N.; Han, D.; Wang, P.; Dang, Y.; Xu, P.; Sui, Y.; Wei, Y. Synergistic effect of fluorine doping and oxygen vacancies on electrochemical performance of ZnCo₂O₄ for advanced supercapacitors and Zn-ion batteries. *Acta Mater.* **2023**, *257*, 119190. [CrossRef]
204. Pacchioni, G. Numerical Simulations of Defective Structures: The Nature of Oxygen Vacancy in Non-reducible (MgO, SiO₂, ZrO₂) and Reducible (TiO₂, NiO, WO₃) Oxides. In *Defects at Oxide Surfaces*; Springer International Publishing: Cham, Switzerland, 2015; Volume 58, pp. 1–28. [CrossRef]
205. He, J.; Hu, Z.; Deng, K.; Zhao, R.; Lv, X.; Tian, W.; Zhang, Y.X.; Ji, J. A triple-layered PPy@NiCo LDH/FeCo₂O₄ hybrid crystalline structure with high electron conductivity and abundant interfaces for supercapacitors and oxygen evolution. *CrystEngComm* **2021**, *23*, 2262–2268. [CrossRef]
206. Zheng, J.; Zhang, Y.; Meng, C.; Wang, X.; Liu, C.; Bo, M.; Pei, X.; Wei, Y.; Lv, T.; Cao, G. V₂O₃/C nanocomposites with interface defects for enhanced intercalation pseudocapacitance. *Electrochim. Acta* **2019**, *318*, 635–643. [CrossRef]
207. Wang, P.; Ding, X.; Zhe, R.; Zhu, T.; Qing, C.; Liu, Y.; Wang, H.-E. Synchronous Defect and Interface Engineering of NiMoO₄ Nanowire Arrays for High-Performance Supercapacitors. *Nanomaterials* **2022**, *12*, 1094. [CrossRef] [PubMed]
208. Ranjith, K.S.; Lee, S.-Y.; Ghoreishian, S.M.; Chodankar, N.R.; Rama Raju, G.S.; Patil, S.J.; Huh, Y.S.; Park, S.-J.; Han, Y.-K. Defect and interface engineering of MXene-tagged N,F-doped carbon-CoSe₂ heterostructure for superior hydrogen evolution reactions and supercapacitors. *Carbon* **2023**, *206*, 246–259. [CrossRef]
209. Maria Mahimai, B.; Li, E.; Pang, J.; Zhang, J.; Zhang, J. Interface engineering in conducting polymers-based supercapacitor. *J. Energy Storage* **2024**, *96*, 112598. [CrossRef]
210. Zheng, X.; Jiang, J.; Bi, T.; Jin, F.; Li, M. FeCo₂S₄@Ni@graphene Nanocomposites with Rich Defects Induced by Heterointerface Engineering for High-Performance Supercapacitors. *ACS Appl. Energy Mater.* **2021**, *4*, 3288–3296. [CrossRef]
211. Wu, J.; Huang, F.; Lee, T.; Yan, Y.; Pei, X.; Wang, M.; Gao, S.; Guo, S.; Pan, X.; Wang, P. Interface-Guided Formation of 2D Ultrathin MnO₂ Nanosheets with Abundant Oxygen Defects for High Performance Supercapacitors. *ACS Appl. Energy Mater.* **2022**, *5*, 6962–6969. [CrossRef]
212. Chen, Y.; Yin, Z.; Huang, D.; Lei, L.; Chen, S.; Yan, M.; Du, L.; Xiao, R.; Cheng, M. Uniform polypyrrole electrodeposition triggered by phytic acid-guided interface engineering for high energy density flexible supercapacitor. *J. Colloid Interface Sci.* **2022**, *611*, 356–365. [CrossRef] [PubMed]
213. Zhou, X.; Yue, X.; Dong, Y.; Zheng, Q.; Lin, D.; Du, X.; Qu, G. Enhancing electrochemical performance of electrode material via combining defect and heterojunction engineering for supercapacitors. *J. Colloid Interface Sci.* **2021**, *599*, 68–78. [CrossRef] [PubMed]
214. Zhang, F.; Song, G.; Gandla, D.; Ein-Eli, Y.; Tan, D.Q. Synergy of Oxygen Plasma and Al₂O₃ Atomic Layer Deposition on Improved Electrochemical Stability of Activated Carbon-Based Supercapacitor. *Front. Energy Res.* **2021**, *9*, 653203. [CrossRef]
215. Özge Alaş Çolak, M.; Güngör, A.; Akturk, M.B.; Erdem, E.; Genç, R. Unlocking the full potential of citric acid-synthesized carbon dots as a supercapacitor electrode material via surface functionalization. *Nanoscale* **2024**, *16*, 719–733. [CrossRef]
216. Yang, L.; Zhang, L.; Jiao, X.; Qiu, Y.; Xu, W. The electrochemical performance of reduced graphene oxide prepared from different types of natural graphites. *RSC Adv.* **2021**, *11*, 4042–4052. [CrossRef]
217. Wang, J.; Zhang, C.; Chen, Z.; Dong, J.; Chang, P.; Yang, T.; Zhang, J.; Zhao, P.-Y. An environment-friendly method to prepare fulvic acid-based porous carbon for high energy density supercapacitors. *Diam. Relat. Mater.* **2024**, *149*, 111587. [CrossRef]
218. Zhang, S.; Wang, J.; Wu, R.; Liu, L.; Pan, B.; Liu, C. Structural and corrosion resistance properties of sputtered zirconium nitride thin films as electrode material for supercapacitor. *J. Alloys Compd.* **2022**, *900*, 163506. [CrossRef]
219. Xu, L.; Zhang, Y.; Zhou, W.; Jiang, F.; Zhang, H.; Jiang, Q.; Jia, Y.; Wang, R.; Liang, A.; Xu, J.; et al. Fused Heterocyclic Molecule-Functionalized N-Doped Reduced Graphene Oxide by Non-Covalent Bonds for High-Performance Supercapacitors. *ACS Appl. Mater. Interfaces* **2020**, *12*, 45202–45213. [CrossRef]
220. Fan, Y.-F.; Yi, Z.-L.; Song, G.; Wang, Z.-F.; Chen, C.-J.; Xie, L.-J.; Sun, G.-H.; Su, F.-Y.; Chen, C.-M. Self-standing graphitized hybrid Nanocarbon electrodes towards high-frequency supercapacitors. *Carbon* **2021**, *185*, 630–640. [CrossRef]
221. Garcés, L.; López-Mireles, D.A.; Padmasree, K.P.; Mtz-Enriquez, A.I.; Encinas, A.; Oliva, J. Stretchable supercapacitors made with plasticine/graphene/CeNdNiO₂ composite electrodes. *Mater. Chem. Phys.* **2024**, *313*, 128721. [CrossRef]
222. Lim, T.; Ho, B.T.; Suk, J.W. High-performance and thermostable wire supercapacitors using mesoporous activated graphene deposited on continuous multilayer graphene. *J. Mater. Chem. A* **2021**, *9*, 4800–4809. [CrossRef]
223. Meng, Q.; Du, C.; Xu, Z.; Nie, J.; Hong, M.; Zhang, X.; Chen, J. Siloxene-reduced graphene oxide composite hydrogel for supercapacitors. *Chem. Eng. J.* **2020**, *393*, 124684. [CrossRef]
224. Que, L.; Zhang, L.; Wu, C.; Zhang, Y.; Pei, C.; Nie, F. Pt-decorated graphene network materials for supercapacitors with enhanced power density. *Carbon* **2019**, *145*, 281–289. [CrossRef]

225. Zhang, H.; Yang, D.; Lau, A.; Ma, T.; Lin, H.; Jia, B. Hybridized Graphene for Supercapacitors: Beyond the Limitation of Pure Graphene. *Small* **2021**, *17*, 202007311. [[CrossRef](#)]
226. Mohamed, N.B.; El-Kady, M.F.; Kaner, R.B. Macroporous Graphene Frameworks for Sensing and Supercapacitor Applications. *Adv. Funct. Mater.* **2022**, *32*, 202203101. [[CrossRef](#)]
227. Kim, K.H.; Yang, M.; Cho, K.M.; Jun, Y.-S.; Lee, S.B.; Jung, H.-T. High quality reduced graphene oxide through repairing with multi-layered graphene ball nanostructures. *Sci. Rep.* **2013**, *3*, 3251. [[CrossRef](#)]
228. Chen, K.; Li, Z.; Liu, Q.; Xu, M.; Jiang, Q.; Dong, Z.; Wang, X.; Chen, X.; Li, S.; Gao, F. Graphene/GaN ultraviolet photodetector performance regulated by a HfO_2 insulating layer. *Appl. Phys. Lett.* **2024**, *124*, 052103. [[CrossRef](#)]
229. Yang, F.; Zhang, L.; Zuzuarregui, A.; Gregorczyk, K.; Li, L.; Beltrán, M.; Tollar, C.; Brede, J.; Rogero, C.; Chuvalin, A.; et al. Functionalization of Defect Sites in Graphene with RuO_2 for High Capacitive Performance. *ACS Appl. Mater. Interfaces* **2015**, *7*, 20513–20519. [[CrossRef](#)]

Disclaimer/Publisher's Note: The statements, opinions and data contained in all publications are solely those of the individual author(s) and contributor(s) and not of MDPI and/or the editor(s). MDPI and/or the editor(s) disclaim responsibility for any injury to people or property resulting from any ideas, methods, instructions or products referred to in the content.